THESIS FOR THE DEGREE OF DOCTOR OF PHILOSOPHY

Novel Thermoplastic Material Concepts for High Voltage Cable Insulation

Engineering Immiscible Blends for a Sustainable Future

YINGWEI OUYANG

Department of Chemistry and Chemical Engineering

CHALMERS UNIVERSITY OF TECHNOLOGY

Gothenburg, Sweden 2021

Novel Thermoplastic Material Concepts for High Voltage Cable Insulation
Engineering Immiscible Blends for a Sustainable Future
YINGWEI OUYANG
ISBN 978-91-7905-558-5

Doktorsavhandlingar vid Chalmers tekniska högskola
Ny serie nr 5025
ISSN 0346-718X

Department of Chemistry and Chemical Engineering
Chalmers University of Technology
SE-412 96 Gothenburg
Sweden
Telephone + 46 (0)31-772 1000

Cover:
Illustration of the cross-section of a subsea high voltage cable underwater, featuring the unique microstructure obtained by scanning electron microscopy of one of the ternary blends (*see Chapter 8*) studied in this thesis.

Chalmers Reproservice
Gothenburg, Sweden 2021

Novel Thermoplastic Material Concepts for High Voltage Cable Insulation
Engineering Immiscible Blends for a Sustainable Future

YINGWEI OUYANG
Department of Chemistry and Chemical Engineering
Chalmers University of Technology

ABSTRACT

To cope with our growing demand for energy in a sustainable way, efficient long-distance power transmission via high voltage direct current (HVDC) cables is crucial – these cables facilitate the integration of renewable energy into our power networks. For reliable and efficient power transmission, underground and undersea cables require robust insulation materials that possess a high level of mechanical integrity, a low direct-current (DC) electrical conductivity and a high thermal conductivity at the elevated temperatures experienced during cable operation. There is growing interest in thermoplastic materials that fulfill these requirements since thermoplastics offer the possibility for mechanical recycling by melt-reprocessing, and allow for more energy efficient cable production.

In this thesis, it is shown that thermoplastic blends of low-density polyethylene (LDPE) and isotactic polypropylene (iPP) can be engineered towards HVDC cable insulation applications despite the immiscibility between LDPE and iPP. Reactive compounding was explored as a strategy for compatibilising iPP and LDPE, resulting in a material concept that exhibited good thermomechanical properties while maintaining low DC electrical conductivity and thermoplasticity. Blends comprising iPP, LDPE and a styrenic copolymer were also investigated. This led to another thermoplastic material concept where the blend composition could be tuned to simultaneously attain appropriate mechanical stiffness, DC electrical conductivity and thermal conductivity. Further, the addition of Al_2O_3 nanoparticles was found to reduce the already low DC electrical conductivity of such blends. The novel material concepts described in this thesis may facilitate the design of thermoplastic insulation materials for HVDC cables of the future.

Keywords*: high-voltage power cable insulation, thermoplastic, polymer blends, polyethylene, polypropylene, copolymer.*

Nomenclature

DC	Direct-current
DSC	Differential Scanning Calorimetry
DMA	Dynamic mechanical analysis
HDPE	High density polyethylene
HVDC	High voltage direct current
iPP	Isotactic polypropylene
LDPE	Low-density polyethylene
PE	Polyethylene
PP	Polypropylene
SAXS	Small Angle X-Ray Scattering
SEBS	Polystyrene-*b*-poly(ethylene-co-butylene)-*b*-polystyrene
SEM	Scanning electron microscopy
TMA	Thermomechanical analyser
XLPE	Crosslinked polyethylene
WAXS	Wide Angle X-Ray Scattering

Publications

This thesis consists of an extended summary of the following appended papers:

Paper I **Recyclable polyethylene insulation via reactive compounding with a maleic anhydride-grafted polypropylene,** Yingwei Ouyang, Massimiliano Mauri, Amir Masoud Pourrahimi, Ida Östergren, Anja Lund, Thomas Gkourmpis, Oscar Prieto, Xiangdong Xu, Per-Ola Hagstrand, Christian Müller. *ACS Applied Polymer Materials*, 2020, **2** (6), 2389-2396.

Paper II **High-temperature creep resistant ternary blends based on polyethylene and polypropylene for thermoplastic power cable insulation,** Yingwei Ouyang, Amir Masoud Pourrahimi, Anja Lund, Xiangdong Xu, Thomas Gkourmpis, Per-Ola Hagstrand, and Christian Müller. *Journal of Polymer Science*, 2021, **59** (11), 1084– 1094.

Paper III **Highly insulating thermoplastic blends comprising a styrenic copolymer for direct current power cable insulation,** Yingwei Ouyang, Amir Masoud Pourrahimi, Ida Östegren, Jakob Ånevall, Marcus Mellqvist, Azadeh Soroudi, Anja Lund, Xiangdong Xu, Thomas Gkourmpis, Per-Ola Hagstrand, and Christian Müller. *Manuscript.*

Paper IV **Highly insulating thermoplastic nanocomposites based on a polyolefin ternary blend for HVDC Power Cables,** Azadeh Soroudi, Yingwei Ouyang, Xiangdong Xu, Fritjof Nilsson, Mikael Hedenqvist, and Christian Müller. *Manuscript.*

The author has published the following papers which are not included in the thesis:

Paper V **Click chemistry-type crosslinking of a low-conductivity polyethylene copolymer ternary blend for power cable insulation,** Massimiliano Mauri, Anna I Hofmann, Diana Gómez-Heincke, Sarath Kumara, Amir Masoud Pourrahimi, Yingwei Ouyang, Per-Ola Hagstrand, Thomas Gkourmpis, Xiangdong Xu, Oscar Prieto, Christian Müller, *Polymer International*, 2019, **69**, 404-412.

Paper VI **Electrical characterization of a new crosslinked copolymer blend for DC Cable Insulation,** Sarath Kumara, Xiangdong Xu, Thomas Hammarström, Yingwei Ouyang, Amir Masoud Pourrahimi, Christian Müller and Yuriy V. Serdyuk, *Energies*, 2020, **13**, 1434.

The author of this thesis is also an inventor of the following patent applications:

Patent I **Polymer composition for cable insulation (EP3739001A1)**. Yingwei Ouyang, Thomas Gkourmpis, Per-Ola Hagstrand, Christian Müller. *Published 2020.*

Patent II **Polymer compositions comprising mixtures of polyolefins (WO2020229657A1)**. Yingwei Ouyang, Massimiliano Mauri, Thomas Gkourmpis, Per-Ola Hagstrand, Oscar Prieto, Denis Yalalov, Christian Müller. *Published 2020.*

Patent III **Composition (EP3739597A1)**. Yingwei Ouyang, Massimiliano Mauri, Thomas Gkourmpis, Per-Ola Hagstrand, Oscar Prieto, Denis Yalalov, Christian Müller. *Published 2020.*

Patent IV **Compositions comprising LDPE, polypropylene and functionalised polyolefins (WO2020229658A1)**. Yingwei Ouyang, Thomas Gkourmpis, Per-Ola Hagstrand, Oscar Prieto, Denis Yalalov, Christian Müller. *Published 2020.*

Contribution Report

Paper I — Main author. Together with M. Mauri and C. Müller responsible for concept of the work and the design of experiments. Responsible for all sample preparation, data collection using thermal and thermomechanical methods, SEM imaging, shear rheometry and infrared spectroscopy. Electrical conductivity measurements were performed by A. M. Pourrahimi. Responsible for data analysis. The first draft of the manuscript was written together with C. Müller. Revised manuscript with all co-authors.

Paper II — Main author. Together with C. Müller, T. Gkourmpis and P.-O. Hagstrand, responsible for concept of the work and the design of experiments. Responsible for all sample preparation, data collection using thermal and thermomechanical methods, and SEM imaging. A. M. Pourrahimi performed electrical conductivity measurements and A. Lund conducted X-ray scattering experiments. Responsible for data analysis. The first draft of the manuscript was written together with C. Müller. Revised manuscript with all co-authors.

Paper III — Main author. Together with C. Müller and P.-O. Hagstrand responsible for concept of the work and the design of experiments. Responsible for sample preparation, data collection using thermal and thermomechanical methods, thermal conductivity measurements, SEM imaging, shear rheometry. A. M. Pourrahimi performed electrical conductivity measurements and I. Östergren conducted X-ray scattering experiments. J. Ånevall and M. Mellqvist assisted with sample preparation and thermomechanical characterisation. Responsible for data analysis. The first draft of the manuscript was written together with C. Müller. Revised manuscript with all co-authors.

Paper IV — Co-author. Together with C. Müller and A. Soroudi responsible for concept of the work and the design of experiments. Responsible for SEM imaging. Sample preparation, data collection using thermal and thermomechanical methods, and electrical conductivity measurements, were done by A. Soroudi. I. Östergren conducted scattering experiments. Together with A. Soroudi responsible for data analysis. The first draft of the manuscript was written by A. Soroudi and C. Müller. Revised manuscript with all co-authors.

TABLE OF CONTENTS

Chapter 1

Towards a Sustainable Future

As we observe and experience the effects of global warming and pollution, it is clear that living the way we do now is unsustainable. Urgent changes are necessary to ensure that the needs of the present are met 'without compromising the ability of future generations to meet their own needs'.[1] This is the definition of sustainable development, first introduced by the World Commission on Environment and Development (WCED) in 1987.[1] There are three interconnected pillars of sustainability – environmental, social and economic.[2] These have been the basis of the 17 Sustainable Development Goals (SDGs) laid out by the United Nations (UN) as part of the 2030 Agenda for Sustainable Development.[3] Sustainability is a multi-faceted topic. Even within the environmental category, there are several SDGs including 'Affordable and Clean energy', 'Responsible Consumption and Production', 'Climate Action', 'Life below Water' and 'Life on land',[3] reflecting the multitude of considerations we need to take into account in order to achieve environmental sustainability.

High voltage direct-current (HVDC) cables play an important role in tackling the SDGs 'Affordable and Clean Energy' and 'Climate Action' – they enable efficient electrical transport over long distances, which facilitates our shift away from fossil fuels towards sources of renewable energy (see chapter 2).[4-6] HVDC cable technologies can further contribute to a more sustainable future if other SDGs such as 'Responsible Consumption and Production' are also taken into account. This can be achieved if the environmental impact associated with the cables before, during and at the end of their lifetime, are identified and mitigated as much as possible.

With regard to the environmental impact of cable manufacturing, aspects such as sourcing and transportation of raw materials, processing and cable installation should be considered. In the ideal scenario, raw materials and energy (for material transportation and manufacturing) will be derived from sustainable sources, processes will be energy efficient, and the overall carbon footprint will be low. Waste will also be minimal, non-toxic, and handled appropriately so as not to harm the environment.

With regard to the usage phase, we should aim for high cable efficiency and reliability over long times (cable lifetime currently ~50 years[7]). By engineering the materials and designs for cables for high performance and durability, we can maximise the benefits we reap from our investment in materials and energy for manufacturing. Furthermore, since HVDC cables are buried underground or laid undersea,[4, 8, 9] cables should also be designed to minimise negative impacts on organisms living where cable infrastructures are implemented.[10]

At the end of life of the cable, it would be ideal if as much material as possible can be extracted from the cable and recycled into high quality products via energy-efficient processes. Materials that cannot be recycled should then be disposed of appropriately to minimise any negative impact on the environment.

While I have described ideal-case scenarios for cables in terms of sustainability, these are hard to achieve fully. In reality, materials, processes, designs and technologies are engineered such that the advantages outweigh the disadvantages. Nonetheless, we should strive towards maximising the positives and eliminating negatives. Therefore, I have explored new material concepts for HVDC cable insulation in my PhD work, aiming not only towards more efficient power transmission for our transition towards renewable energy, but also more energy efficient cable manufacturing and insulation materials that can be mechanically recycled by melt-reprocessing.

Chapter 2

Why High Voltage Direct Current (HVDC) Cables?

2.1 The energy problem

The World Energy Council predicts that compared to 2010, the global energy consumption will increase by at least 35% in 2030.[11] By 2035, the annual consumption is projected to reach around 778 Etta Joule.[12] To sustainably cope with our growing demand for energy, renewable energy technologies and energy efficiency are key.[13-15] Our diversion from fossil fuels to renewables is not only crucial to prevent finite resources from being consumed at unsustainable rates, but also to combat climate change.[16-18] The fact that two-thirds of all greenhouse gases arise from energy-related carbon dioxide (CO_2) emissions[19] highlights that the transition towards renewables is crucial for reducing greenhouse gas emissions. A significant and rapid reduction in emissions is needed to limit the increase in average global surface temperature (from pre-industrial levels) to well below 2 °C.[13]

2.2 HVDC power cables – an important part of the solution

To phase out fossil fuels as our source of electrical energy, we need technologies not only for harnessing renewable energy[18, 20] but also for energy storage[21-23] and power transmission.[24-26] Renewable energy sources are often intermittent[21-23] and the required infrastructures (e.g. solar and wind farms) are often located far away from populated areas. To ensure a reliable supply of energy, extended power grids that connect these infrastructures and populated areas are necessary.[27, 28] This can be achieved with high voltage direct-current (HVDC) cables, which allow electricity to be transported over long distances of up to a few thousand kilometres with minimal losses.[24]

2.3 HVDC cable design and manufacturing

For efficient power transmission, underground and undersea (necessary for traversing large bodies of water) HVDC cables require robust insulation around their conductors. The two main types of insulated HVDC cables are lapped and extruded cables.[26] Examples of the former include oil-paper insulation, where the conductor is wrapped with paper impregnated with dielectric fluids,[4, 26] and paper-polypropylene laminate (PPL) insulation, where the conductor is wrapped with alternating layers of polypropylene and impregnated paper.[4, 29] Extruded cables on the other hand are insulated by a polymeric layer that surrounds the conductor[26] (Figure 1). As the name suggests, these cables are manufactured by extrusion, where molten polymeric insulation material is extruded directly onto the conductor and deposited as a compact and uniform layer (along with the semiconducting layers that are also extruded) around the conducting core.[4] To achieve high transmission voltages, extruded cables are generally preferred over lapped insulation cables due to their ability to withstand higher conductor temperatures that allow for higher transmission capacity,[4, 8, 30] simpler jointing procedures, reduced weight, and the elimination of environmental concerns over oil leakages.[4, 26, 30, 31] Hence, significant research and development efforts have been invested in extruded cable technologies.

Figure 1. Schematic showing the cross-section of a typical underground extruded HVDC cable, where the semiconducting layers smoothen the electric field,[4, 32, 33] the metallic screen controls the shape of the electric field,[4] contains the electric field within the cable[34] and offers mechanical support,[4] and the outer sheath protects the cable from external forces.[4, 10, 33]

2.4 Extruded HVDC cables based on XLPE

Currently, the most widely-used type of extruded HVDC cables are those insulated with crosslinked polyethylene (XLPE).[26, 30, 35, 36] The base resin of XLPE is low density polyethylene (LDPE), which can be produced with very high chemical and physical cleanliness.[37] This material offers very low DC electrical conductivity,[38] an adequate thermal conductivity, good mechanical flexibility even at low temperatures[39, 40] and good processability for melt extrusion,[36, 40] making it an excellent candidate for HVDC cable insulation. However, the melting temperature of LDPE is too low, resulting in inadequate mechanical stability at high cable operating temperatures.[33, 41] Therefore, LDPE is crosslinked to form XLPE, which not only has good electrical properties,[36, 37, 42] but also features thermomechanical properties[36, 42] that allow the material to function at typical cable operating temperatures of 70-90 °C.[36, 38, 40, 43, 44] Thanks to recent developments in XLPE-based HVDC cable technology, commercial transmission lines can now reach voltages as high as 640 kV and can transmit at least 3 GW of electrical power.[24]

Chapter 3

New Developments for HVDC Cable Insulation: Thermoplastics and Higher Operating Temperatures

3.1 Material requirements

Efficient and reliable electrical transport over long distances requires HVDC cables with robust insulation materials. As we strive towards cables with increased transmission capacity, it is necessary to develop insulation materials that can support increasingly high voltages.[45-47] Although a higher current as well as voltage can increase electrical power, the latter is favoured because an increase in current is accompanied by more substantial Joule heating.[46, 47] However, higher voltages have other implications. For an insulation layer of a given thickness, higher voltages will result in higher electric fields, leading to a higher DC electrical conductivity of the insulation, and hence an increase in leakage current. This can lead to a temperature rise, which in turn further increases the DC electrical conductivity that yet again contributes to even more heating. This process of thermal runaway would ultimately lead to electrical breakdown.[48] Hence the insulation material must possess a sufficiently low DC electrical conductivity to keep leakage current heating under control. Further, it is also of benefit if the insulation material has a high thermal conductivity to facilitate heat dissipation away from the conductor to prevent build-up of thermal hotspots, which increase the probability of thermal breakdown.[24, 49, 50] Moreover, high thermal conductivity will in principle contribute to a lower conductor temperature, leading to lower conductor losses.

The insulation material must also demonstrate good thermomechanical properties to resist deformation under stresses from the weight of the conducting core and other external forces, especially at the elevated temperatures experienced by the cable. Cable operating temperatures of up to 70-90 °C are common for XLPE cables,[4] and emergency conditions such as power surges and lightning strikes can temporarily heat the cable to much higher temperatures.[4]

3.2 Thermoplastic insulation materials

There has been growing interest in thermoplastic alternatives for high voltage cable insulation[51] due to the benefits that thermoplastics can offer both for cable manufacturing and with regard to sustainability aspects.[52] In fact, commercial products are now available – the first thermoplastic-insulated HVDC cables (from Prysmian Group) will be installed in Germany.[53, 54]

Thermoplastic alternatives to XLPE eliminate the need for peroxide crosslinking (the conventional method for producing XLPE for HVDC cables) by incorporating higher-melting polymer crystals, which can result in improved thermomechanical properties compared to LDPE at temperatures above T_m^{LDPE} (sections 3.2.1 to 3.2.3).[41, 55] Without crosslinking, cable production can be more energy efficient since the crosslinking step (Figure 2) and the byproduct-removing degassing step[40, 48, 52] are omitted. Further, scorch, i.e. premature crosslinking,[56, 57] which can give rise to defects in the insulation material that compromise its quality and reliability,[52, 57] is avoided. This can allow for greater efficiency in cable manufacturing[51] for example by having longer production times since the extruder used for production needs to be cleaned less frequently.[48]

In addition to energy efficiency, thermoplastics are advantageous from a sustainability viewpoint because of the absence of crosslinking byproducts that can be harmful to health and the environment,[48] and the possibility to recycle the insulation material the end of

life of the cable by remelting.[48] This is the conventional way of mechanically recycling polymers.[58] However, it should be noted that mechanical recycling of XLPE is also possible, not by remelting, but by grinding into powder that can be added to virgin thermoplastics,[59-63] or by thermoplasticising using high temperature shearing,[61, 64, 65] but the latter is energy intensive due to the high temperatures used (> 200 °C).[61]

Some PP-based thermoplastic polymer blends can withstand even higher temperatures[41, 48, 66, 67] than XLPE (70-90 °C), such as the insulation currently used in Prysmian's medium voltage alternating current cables (up to 110 °C).[68] With further research, similar material concepts could potentially facilitate the development of thermoplastic insulation materials for HVDC cables that can tolerate even higher operating temperatures than existing extruded HVDC cables,[69] and hence transmit more electrical power. With the appropriate blend composition and processing conditions, thermoplastic materials can be engineered for dimensional stability above T_m^{LDPE}. The stiffness of a material can be described by the storage modulus *E'*, which is typically measured as a function of temperature using dynamic mechanical analysis (DMA). In case of XLPE, a large fraction of LDPE crystals melt at T_m^{LDPE} ~ 110 °C, resulting in a drastic drop in *E'*, yet XLPE maintains *E'* ~ $2 \cdot 10^5$ to $4 \cdot 10^5$ Pa above T_m^{LDPE} due to the presence of chemical crosslinks. *E'* remains almost constant from 120 °C up to 200 °C because of the crosslinks that stay intact until XLPE starts to degrade (Figure 3). Compared to XLPE, thermoplastic alternatives to XLPE can offer an even higher *E'* above T_m^{LDPE}, and the temperature window across which high *E'* is exhibited can be tuned. Furthermore, suitable thermoplastic alternatives would melt completely (drastic modulus drop at T_m) at temperatures well below their degradation temperature (Figure 3), making mechanical recycling by melt-reprocessing possible.

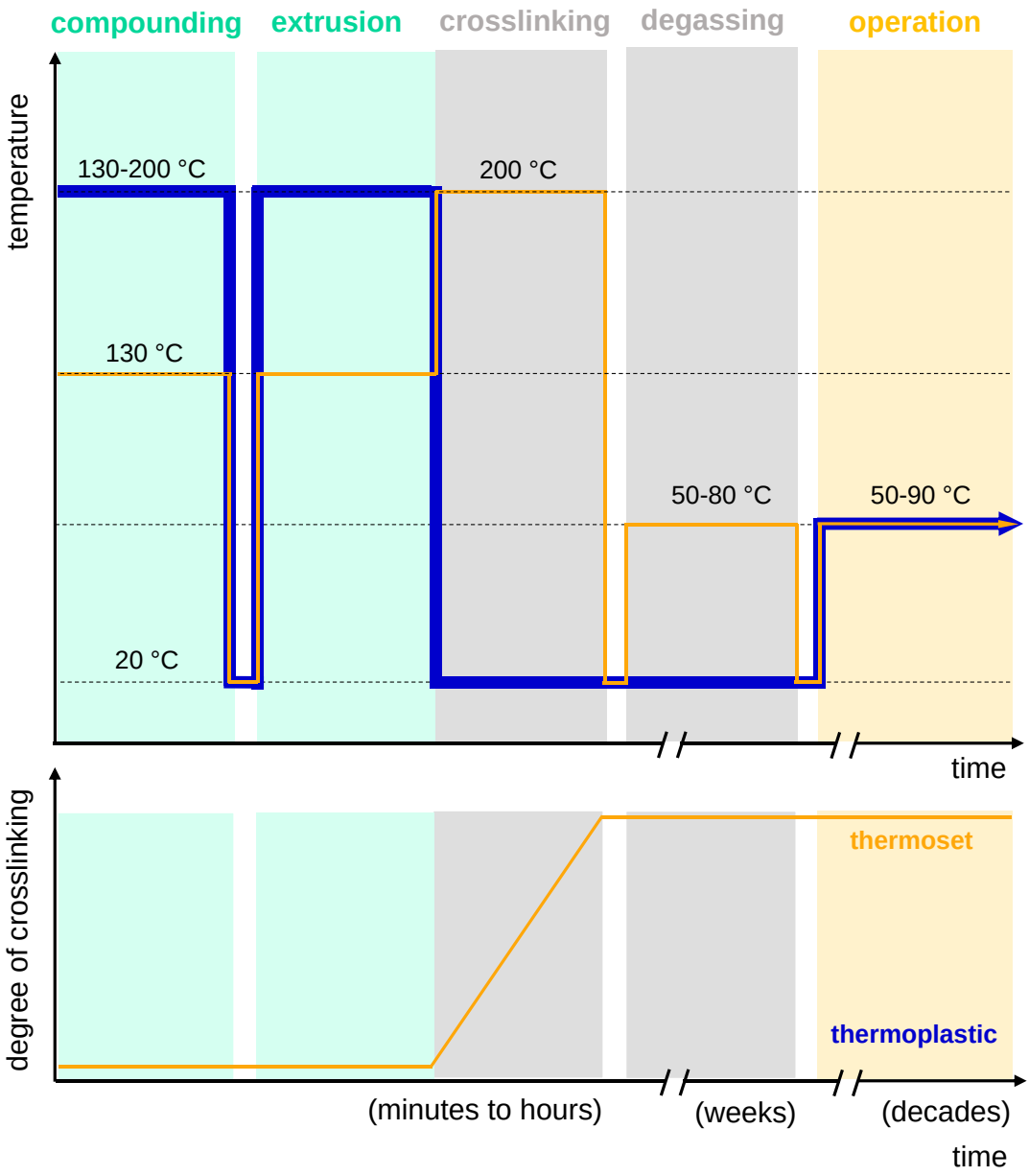

Figure 2. Schematic of the experienced temperature and degree of crosslinking of a traditional *thermoset* cable insulation material (orange line) and a *thermoplastic* insulation material (blue line) during compounding and extrusion (green), the heat activated crosslinking and degassing steps (grey), which are absent for the thermoplastic material, and operation (yellow). *This figure is adapted from Figure 1 of paper I.*

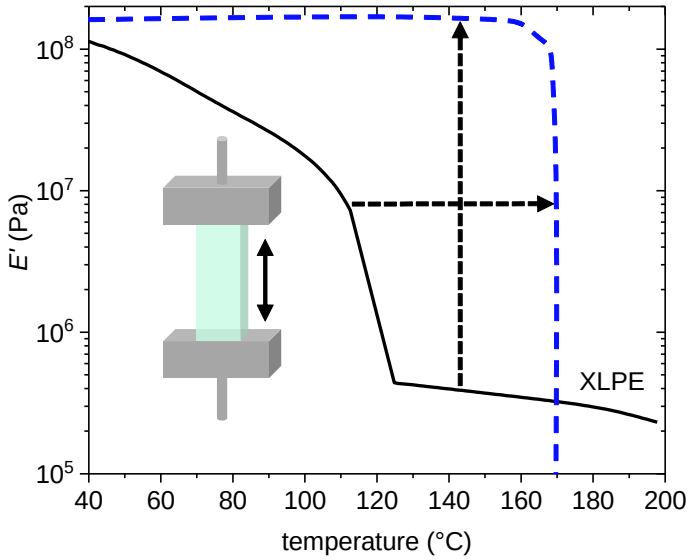

Figure 3. Storage modulus *E'*, which relates to material stiffness, measured with dynamic mechanical analysis (DMA) as a function of temperature of XLPE, i.e. LDPE crosslinked with 1 wt% DCP at 200 °C (black line, data from *paper I*) and an example of an envisioned ideal thermoplastic alternative (blue dashed line) showing how the thermomechanical properties of XLPE can be surpassed by increasing the temperature at which materials soften beyond T_m^{LDPE} (black horizontal dashed line) and/or increasing the stiffness of materials above T_m^{LDPE} (black vertical dashed line), while featuring a drastic drop in modulus at 160 °C for instance, allowing processing at temperatures that are not excessively high (prevents degradation and lowers energy consumption; cf. Figure 2) and reprocessing in the melt (for mechanical recycling); inset: schematic of the oscillatory DMA measurement indicating the direction of applied stress.

3.2.1 Polyethylene blends

Blends comprising LDPE and high-density polyethylene (HDPE) have been studied as potential candidates for HVDC cable insulation.[70-75] HDPE has a melting temperature T_m^{HDPE} ~ 130 °C (cf. 110 °C for LDPE).[70, 76] Since some HDPE and LDPE grades are melt-miscible,[70, 77, 78] good dispersion of HDPE in LDPE can be achieved and LDPE/HDPE co-crystals can form.[70] With appropriate blend compositions, degree of branching of LDPE,

polymer molecular-weight distribution and processing conditions,[70, 79-81] HDPE:LDPE blends can display a higher *E'* than LDPE above T_m^{LDPE} due to the presence of HDPE crystals and LDPE:HDPE co-crystals.[70] These crystals, connected by tie chains, act as network points together with trapped entanglements to form a network that extends across the material, holding the material together under stress in the temperature range $T_m^{LDPE} < T < T_m^{HDPE}$.[70]

HDPE is polymerised with transition metal catalysts in low pressure reactors.[82] Remaining catalyst residues are thought to compromise the cleanliness and hence DC dielectric properties of linear polyethylenes. Hence, Andersson et al. explored HDPE:LDPE blends with a low HDPE content. Adding as little as 1-2 wt% HDPE was sufficient to arrest creep at 115 ˚C, i.e. above T_m^{LDPE}, when subjected to 1 kPa stress (~1x sample weight).[70] Further, a blend with just 1 wt% HDPE was reported to have a DC conductivity of σ_{DC} ~ 10^{-15} S m^{-1} at high electric fields of 30 and 40 kV mm^{-1} at 70 °C. This value is roughly one order of magnitude lower than σ_{DC} of both XLPE and LDPE.[38]

3.2.2 Polypropylene-based materials

Although HDPE:LDPE blends display good potential for use as HVDC insulation, materials that can maintain structural integrity well above T_m^{HDPE} would provide additional advantages. Polypropylene-based materials have therefore gained significant attention,[51, 66, 83-89] and first commercial products for HVDC cable insulation have been developed.[53, 54, 90] The main advantage of PP is its high melting temperature,[41, 55] which is as high as T_m^{PP}~170 °C for isotactic polypropylene (iPP).[85, 91] Further, iPP can be produced with a high degree of intrinsic cleanliness and displays very low DC electrical conductivity[55] as low as σ_{DC} ~ 10^{-15} S m^{-1} at high electric fields.[91] Hence, iPP is widely used for the manufacture of dielectric films for capacitors.[55] However, the main drawback of neat iPP is its mechanical properties at low temperatures.[55, 67] iPP is too brittle[41] below its T_g ~ 0 °C[92] and too stiff at low

temperatures,[51, 67] which complicates the laying of cables. To obtain polypropylene-based materials that have sufficient mechanical flexibility and toughness at low temperatures, several material concepts have been explored. Syndiotactic polypropylene (sPP), for instance, displays good dielectric properties and thermal stability, and is mechanically flexible due to its small spherulites and low crystallinity.[88] The main drawback of sPP is its high cost.[4, 35] Alternatively, polypropylene copolymerised with comonomers (eg. ethylene, butylene),[67, 87, 93] and blends comprising PP or PP copolymers (eg. LDPE:PP-copolymer, iPP:polyolefin copolymers, PP-copolymer:polyolefin copolymers, iPP:sPP)[66, 83-86, 89, 94, 95] have been explored.

3.2.3 Polyethylene:polypropylene blends

In addition to the above-mentioned material concepts, blends containing iPP and LDPE have been studied for HVDC cable applications.[91, 96, 97] Such materials allow to combine good low-temperature mechanical properties, low DC electrical conductivity and adequately high thermal conductivity of LDPE, with the high-temperature mechanical stiffness and very low DC electrical conductivity of some iPP grades. However, due to the immiscibility between iPP and LDPE,[98, 99] the two polymers strongly phase separate. Hence, connectivity of the minor phase is difficult to achieve. To reinforce LDPE with iPP, the iPP phase should be continuous. There is a critical composition where the LDPE and iPP phases are co-continuous. This can be achieved by tuning the blend composition and/or viscosity ratios of the components based on the relation $\frac{\eta_{LDPE}}{\eta_{PP}} = \frac{\emptyset_{LDPE}}{\emptyset_{PP}}$ for a given shear rate, where η is the viscosity and $\emptyset$ is the volume fraction.[100] Co-continuous iPP and LDPE phases are observed in the 40:60 iPP:LDPE blend (Figure 4). Continuity of the iPP phase in iPP:LDPE blends has been shown to be necessary for achieving a high *E'* at T > T_m^{LDPE} (Figure 5). While blends with high iPP content offer a high degree of dimensional stability at elevated temperatures and a low DC electrical conductivity, they are stiffer than XLPE below T_m^{LDPE} (Figure 5), and feature a low thermal conductivity (see

chapter 6 and 8 for characterisation of neat iPP and iPP:LDPE blends, respectively). It can be anticipated that such systems require effective compatibilisation to facilitate iPP dispersion in LDPE-rich blends, necessary for obtaining improved thermomechanical properties such as a high *E'* at T > T_m^{LDPE}, without incorporating too much iPP that will be detrimental for the low-temperature mechanical properties and thermal conductivity of iPP:LDPE blends.

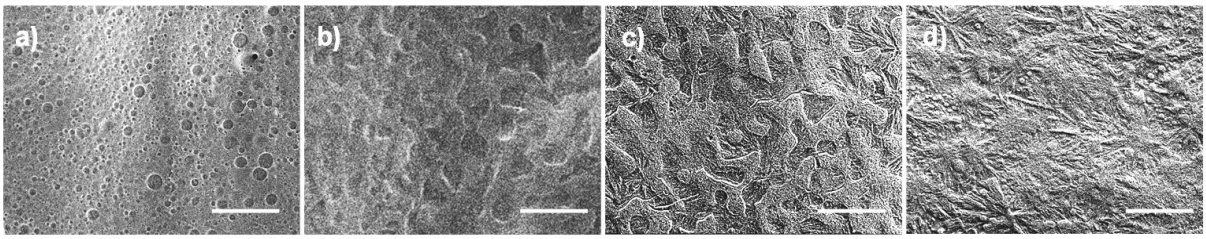

Figure 4. Scanning electron microscopy (SEM) micrographs of cryofractured, etched and sputtered surfaces of iPP:LDPE blends with iPP content: **(a)** 20 wt% **(b)** 40 wt%, **(c)** 60 wt%, and **(d)** 80 wt% (scale bar = 20 µm). (taken from Figure 4 of *paper II*, with corrected scale)

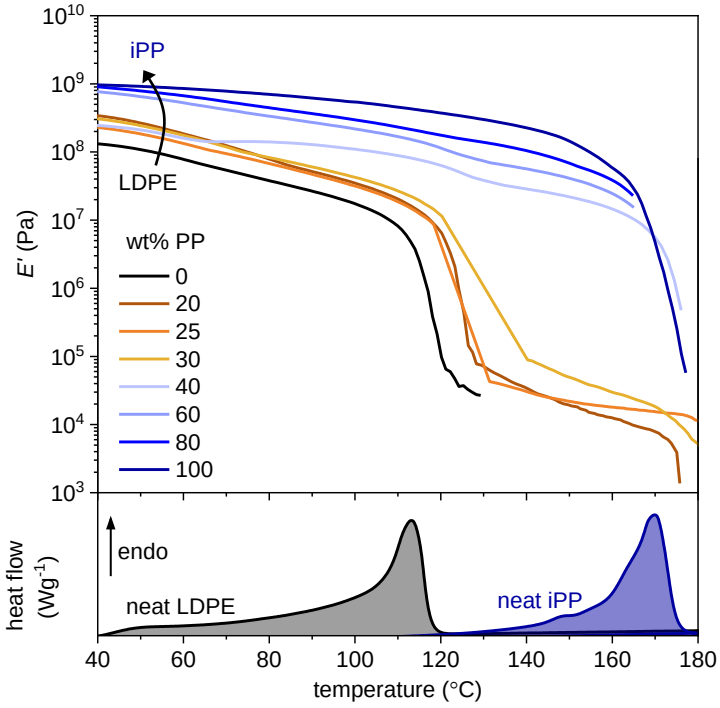

Figure 5. Top: storage modulus *E'* measured with DMA as a function of temperature of neat LDPE (black), neat iPP (navy), iPP:LDPE blends containing 20 to 30 wt% iPP (shades from brown to yellow) and 40 to 80 wt% iPP (shades of blue); bottom: differential scanning calorimetry (DSC) first heating thermograms of neat LDPE (black) and neat iPP (navy).

Chapter 4

Project Aim

The overall goal of the project is to develop new material concepts for high voltage cable insulation that demonstrate 1) excellent thermomechanical properties, 2) a low DC electrical conductivity, 3) an adequate thermal conductivity and 4) thermoplastic behaviour. This thesis focuses on blends based on LDPE and iPP, and explores routes towards materials that possess the property portfolio needed for insulating HVDC cables of the future.

Chapter 5

Materials and Methods

5.1 Materials

LDPE with MFI ~ 2 g/10 min (190 °C / 2.16 kg), M_n ~ 13 kg mol^{-1}, PDI ~ 9 and number of long-chain branches ~ 1.9 per 1000 carbons (characterisation reported in ref. 38), was obtained from Borealis AB. (*Paper I-IV*)

XLPE was prepared from LDPE infused with 1 wt% dicumyl peroxide (DCP) (see section 5.2.1 for experimental procedure for crosslinking and subsequent degassing) (*Paper I-II*)

LDPE:Al_2O_3 masterbatch containing 3 wt% Al_2O_3 nanoparticles, 97 wt% LDPE and 0.02 wt.% Irganox 1076 was provided by Fritjof Nilsson (KTH). The Al_2O_3 nanoparticles used had an average diameter of (50 ± 25) nm, and they were surface-modified with n-octyltriethoxysilane (*Paper IV*)

Isotactic polypropylene (iPP) with M_n ~ 40 kg mol^{-1}, M_w ~ 348 kg mol^{-1}, PDI ~ 8.6 and isotacticity > 90%, was obtained from Borealis Polymers N.V. (*Paper II-IV*)

Random heterophasic polypropylene (hPP), composed of random propylene-ethylene copolymers and contains 40% of an ethylene-rich rubbery phase dispersed in a propylene-rich matrix, was obtained from Borealis AB. (*Chapter 6,10*)

Branched statistical ethylene-glycidyl methacrylate copolymer p(E-*stat*-GMA) with a GMA content of 4.5 wt%, a melt flow index MFI ~ 2 g/10 min (190 °C / 2.16 kg), and a density of 0.93 g cm^{-3} was obtained from Arkema (Lotader series AX8820). (*Paper I*)

Isotactic polypropylene-maleic anhydride graft copolymer iPP-*graft*-MA with a MA content of 8 - 10 wt%, a density of 0.93 g cm^{-3}, number-average molecular weight M_n ~ 4 kg mol^{-1} and PDI ~ 2.3 was obtained from Sigma Aldrich (product number 427845). (*Paper I*)

Polystyrene-*b*-poly(ethylene-*co*-butylene)-*b*-polystyrene (SEBS):

$SEBS_A$ with a melt-flow index of MFI ~ 2 - 4.5 g/10 min (230 °C / 2.16 kg) and 11.5 - 13.5 % polystyrene content was obtained from Kraton Corporation (Kraton G1645 MO). (*Paper II*)

$SEBS_B$ with MFI < 1 g/10 min (230 °C / 2.16 kg) and 18.5 - 22.5 % polystyrene content was obtained from Kraton Corporation (Kraton G1642 HU). (*Paper III & IV*)

5.2 Methods

5.2.1 Sample preparation

Compounding of most blends was done by recirculation for the desired compounding time (5 - 15 minutes) at selected temperatures (170 - 220 °C) with a screw speed of 50 rpm in an Xplore Micro Compounder MC5 (~ 2.5 g) followed by extrusion. Upscaled $SEBS_B$:iPP:LDPE ternary blends (~ 2 kg) were compounded at 120 rpm at temperatures up to 200 °C in a Coperion ZSK 26 K 10.6 twin screw extruder, followed by extrusion. Plates were prepared by heating the extrudates to 170 °C or 200 °C and melt-pressing for 1 - 3 minutes in a hot press before cooling (see experimental section of individual papers for specific processing conditions for different blends). Samples for DSC, rheometry, DMA and creep, SEM, WAXS and SAXS measurements were cut from 1.25 mm thick plates, and from 0.3 mm and 4.6 mm plates for DC electrical conductivity and thermal conductivity measurements, respectively.

To prepare XLPE, milled LDPE was dispersed in a solution of DCP in methanol at 40 °C and stirred for 1 h, followed by solvent evaporation. The resulting milled LDPE infused with 1 wt% DCP was melt-pressed at 120 °C for 5 minutes in a hot press. The temperature was then increased to 180 °C, where the sample was left to crosslink for 10 minutes before cooling. This XLPE sample was finally degassed in a vacuum oven at 50 °C overnight.

Al_2O_3 nanocomposites were prepared from the LDPE:Al_2O_3 masterbatch. To prepare this masterbatch, Al_2O_3 nanoparticles with an average diameter of (50 ± 25) nm were surface-modified with n-octyltriethoxysilane according to a previously described procedure.[76] After surface modification, the nanoparticles were dried for 20 h at 80 °C in a vacuum oven and then dispersed in n-heptane (0.3 ml n-heptane per 1g polymer) through ultrasonication for 5 minutes, followed by the addition of Irganox 1076 and LDPE, resulting in a solid content of 3 wt% surface-modified Al_2O_3 nanoparticles, 97 wt% LDPE and 0.02 wt% Irganox 1076. The LDPE:nanoparticle slurry was shaken for 1h and dried overnight at 80 °C. The dried powder was shaken for another 30 minutes, then compounded for 6 minutes at 150 °C and 100 rpm with an Xplore Micro Compounder MC5. The LDPE:Al_2O_3 extrudate was cut into 2-3 mm long granules. Neat LDPE, LDPE nanocomposites, ternary blends and ternary blend nanocomposites were prepared by compounding different amounts of $SEBS_B$, iPP, LDPE and the LDPE:Al_2O_3 masterbatch (dried for 17 h at 80 °C in a vacuum oven) with an Xplore Micro Compounder MC5 under N_2 gas for 4 minutes at 200 °C and 70 rpm followed by extrusion using a die temperature of 210 °C. Extrudates were melt-pressed into 0.3 mm thick films for electrical measurements and 1.9 mm thick films for mechanical analysis using a LabPro 200 Fontijne press at 200 °C for 1 minute followed by cooling at a rate of -10 °C min^{-1}.

5.2.2 Thermomechanical properties

5.2.2.1 Dynamic mechanical analysis (DMA)

Dynamic mechanical analysis (DMA) was the main method of assessing the thermomechanical properties of materials studied in this thesis. Variable temperature DMA thermograms were recorded using a TA Q800 DMA in tensile mode (see experimental section in papers for details). In these experiments, each sample was subjected to an oscillating force and the resulting sinusoidal strain of the sample was measured by the instrument.[101, 102] From these measurements, the storage modulus *E'* of materials as a function of temperature was obtained. This allows to compare the stiffness of different materials at different temperatures, for instance between LDPE and XLPE above T_m^{LDPE} (Figure 6).

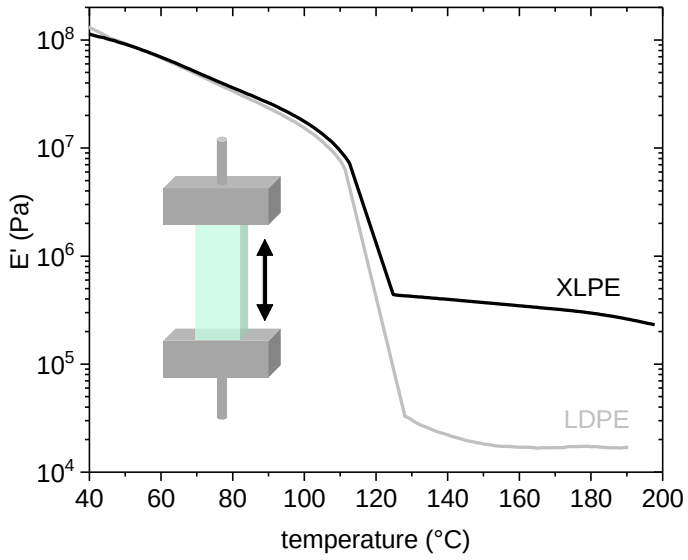

Figure 6. Storage modulus *E'*, measured with dynamic mechanical analysis (DMA) as a function of temperature of XLPE (black line) and LDPE (grey).

5.2.2.2. High-temperature creep tests

Creep tests were conducted using a TA Q800 DMA in tensile mode (see experimental section of papers for details on experimental conditions). For XLPE insulation materials, Hot Set tests are typically done to determine the degree of crosslinking,[48, 103, 104] since the number of crosslinks relates to the material's ability to resist deformation (elongation) under mechanical stresses at high temperatures.[104, 105] Like the Hot Set tests, high-temperature creep tests involve the application of a constant tensile stress to samples at elevated temperatures. The strain, that is the increase in sample length (i.e. elongation) divided by the original sample length, is measured as a function of time. Materials with high dimensional stability at elevated temperatures will arrest creep and show low creep strain (e.g. XLPE), whereas materials with low dimensional stability will elongate rapidly and yield (e.g. LDPE) (Figure 7).

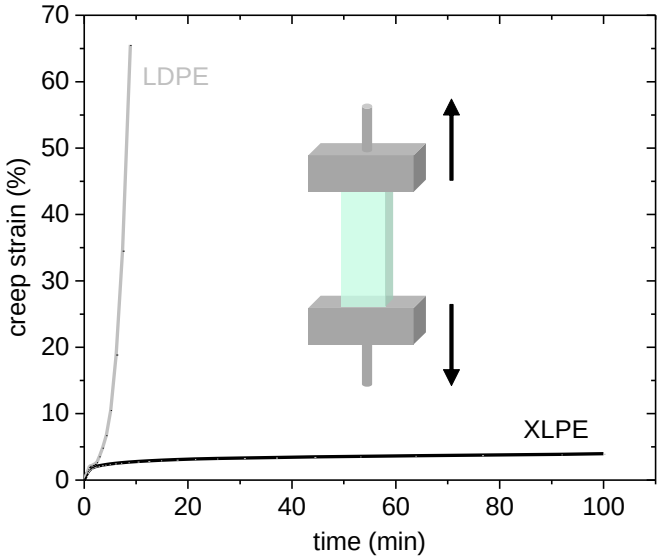

Figure 7. Creep strain at a constant stress of 1 kPa (equivalent to the weight of samples with dimensions 20 mm x 5 mm x 1.3 mm) at 120 °C of LDPE (grey) and XLPE (black) as a function time; inset: schematic of the creep measurement indicating the direction of applied stress.

5.2.2.3. Indentation tests

With the emergence of thermoplastic (i.e. not crosslinked) alternatives, another type of measurement known as the 'thermopressure test' has become more relevant.[48] The thermopressure test mimics the conditions in the cable by simulating the application of an external pressure (eg. a premoulded joint) and assessing the amount of deformation in the relevant temperature window.[48] Therefore, two types of measurements similar to the earlier-mentioned DMA measurements and high-temperature creep tests were performed, but with a compressional force applied instead of tensile force (Figure 8). These indentation tests were conducted using a Thermomechanical Analyser TMA Q400 from TA instruments where force is applied by a glass probe fixed above the sample (details in experimental section of *paper II*).

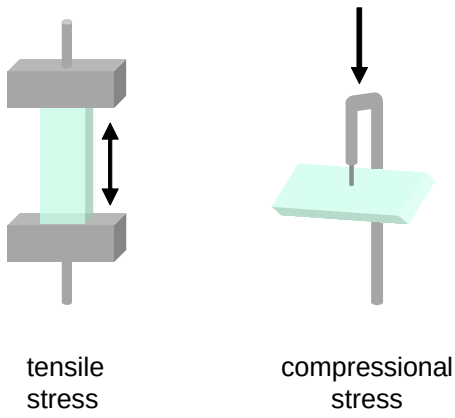

Figure 8. Schematic showing direction of applied tensile stress (left) for experiments done in the DMA, and compressional stress (right) used for indentation tests done in the TMA.

5.2.3. Electrical conductivity

To determine the DC electrical conductivity, sample plates were subjected to an electric field of 30 kV mm^{-1} at 70 °C in a test cell with a three-electrode system setup. The power supply was provided by a Glassman FJ40P03 high-voltage power supplier over at least 18 h, (see experimental section of papers for further details) during which a Keithley 6517B electrometer measured the leakage current. DC electrical conductivity values σ_{DC} of the different materials were calculated from the leakage current after a specified number of hours, using the equation $\sigma_{DC} = \frac{J}{E}$, where J is the current density (i.e. leakage current divided by surface area of the measuring electrode) and E is the electric field.

5.2.4. Thermal conductivity

A Hot Disk 2500 S instrument was used for thermal conductivity measurements, which were performed in an oven at 70 °C (see experimental section of *paper III* for details). For each measurement, a flat Kapton sensor, placed between 2 sample plates, supplied heat over 5 seconds while simultaneously measuring the temperature on the sensor. The Hot Disk software used the change in sensor temperature over time to determine the thermal conductivity of each sample.

Chapter 6

Comparison of Reference Materials: LDPE, XLPE, Random Heterophasic PP and Isotactic PP

The properties of LDPE, XLPE, iPP and a random heterophasic propylene-ethylene copolymer (hPP) are presented to give an idea of material properties to aim towards. XLPE is the benchmark for thermoset HVDC insulation materials, while hPP demonstrates the capabilities of propylene-based thermoplastic alternatives available today.

6.1 Thermomechanical properties

DMA measurements show that XLPE, hPP and iPP feature higher storage moduli than LDPE at $T > T_m^{LDPE}$ up to at least 160 °C (Figure 9). While the rubber modulus of XLPE provides a reference point, a direct comparison of the XLPE thermogram with those of thermoplastic alternatives may not be the most relevant. For instance, the rubber behaviour of XLPE at very high temperatures (e.g. 200 °C) is unnecessary for the application and prohibits reprocessing in the melt (the conventional method for mechanical recycling of plastics). However, as we strive towards materials that do not deform at elevated temperatures, a higher modulus (than XLPE) at temperatures above T_m^{LDPE} would be preferable. The DMA thermogram of hPP shows a material with lower *E'* than iPP at $T < T_m^{LDPE}$ and *E'* that exceeds XLPE at $T_m^{LDPE} < T < T_m^{iPP}$.

Creep tests conducted at 120 °C reveal that XLPE, hPP and iPP effectively arrest creep above T_m^{LDPE} at 120 °C (Figure 10). These materials show very low creep strain < 5% even after 100 minutes, while LDPE elongates rapidly and yields within 10 minutes. Under 1kPa stress at 120 °C (i.e. between T_m^{LDPE} and T_m^{iPP}), the creep deformation of the materials

correlates with their storage moduli in that temperature window measured by DMA. hPP and iPP are even more effective than XLPE at reducing creep strain at temperatures up to their T_m .

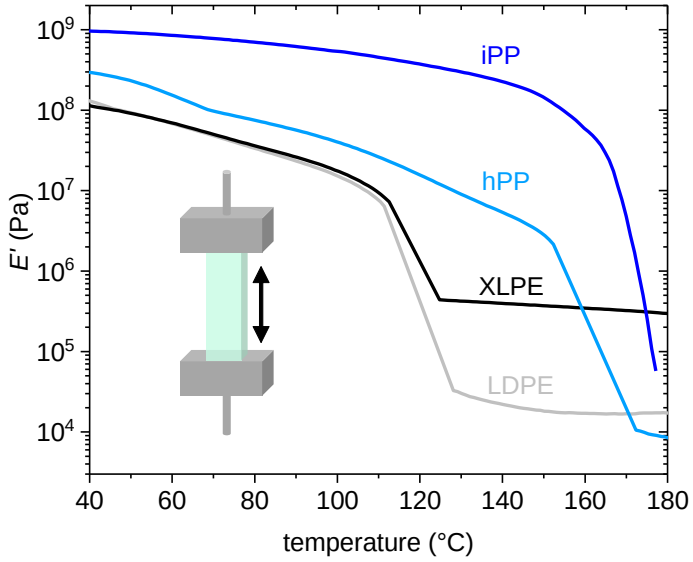

Figure 9. Storage modulus *E'*, measured with DMA as a function of temperature of LDPE (grey), XLPE (black), iPP (blue), and hPP (sky blue).

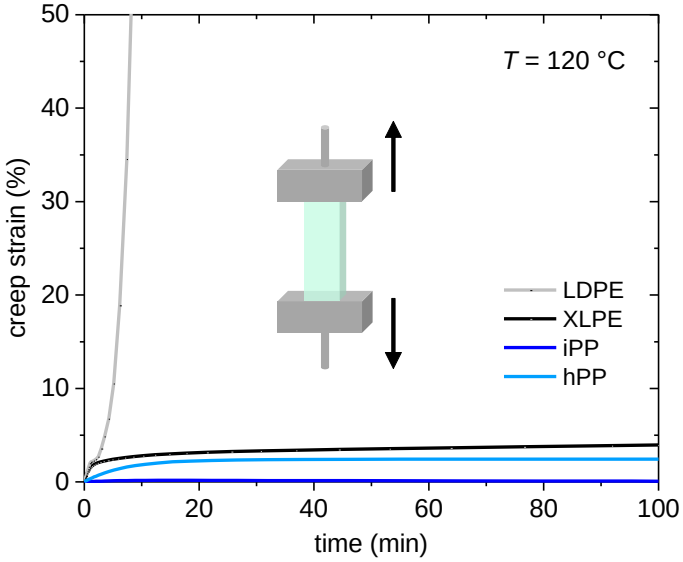

Figure 10. Creep strain at a constant stress of 1 kPa (equivalent to sample weight) at 120 °C as a function of time, of LDPE (grey), XLPE (black), iPP (blue), and hPP (sky blue); inset: schematic of the creep measurement indicating the direction of the applied stress.

6.2 Electrical conductivity

While LDPE and XLPE feature a low DC electrical conductivity in the magnitude of σ_{DC} ~10^{-14} S m^{-1}, iPP and hPP exhibit even lower σ_{DC} values, where iPP exhibits the lowest DC electrical conductivity of σ_{DC} ~$1 \cdot 10^{-15}$ S m^{-1} (Figure 11).

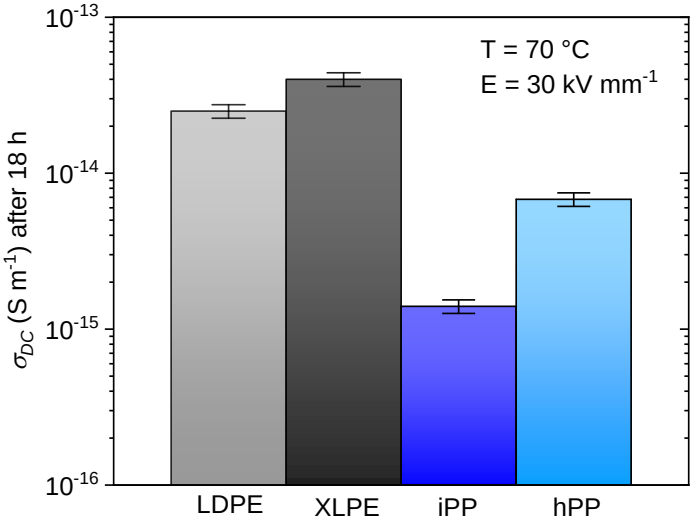

Figure 11. DC electrical conductivity σ_{DC} of LDPE (grey), XLPE (black), iPP (blue), and hPP (sky blue), obtained after 18 h at 70 °C and an electric field of 30 kV mm^{-1}; error bars are based on ~10% error estimated based on three measurements on neat LDPE (data from *paper I*).

6.3 Thermal conductivity

LDPE and XLPE display a higher thermal conductivity κ than iPP and hPP (Figure 12). Higher κ values are favoured for HVDC insulation materials (see Chapter 3). The low κ of propylene-based materials constitutes a major disadvantage and motivates the iPP:LDPE blends that are studied in this thesis.

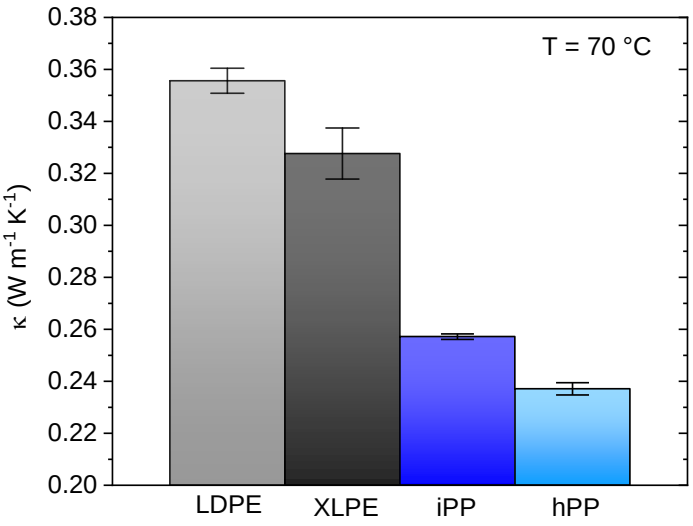

Figure 12. Thermal conductivity κ of LDPE (grey), XLPE (black), iPP (blue), and hPP (sky blue), at 70 °C; error bars are based on the standard deviation calculated from 5 measurements of each sample.

Chapter 7

Compatibilisation through Reactive Compounding

The first material concepts explored in this thesis are based on the reactive compounding of LDPE and iPP via reactive compounding. This involves melt-mixing copolymers of LDPE and iPP that form covalent bonds between their respective functional groups in-situ, ultimately generating LDPE – iPP type copolymers.

7.1 Byproduct-free chemical crosslinking

To eliminate potential byproducts, the branched statistical ethylene-glycidyl methacrylate copolymer (p(E-*stat*-GMA)) and maleic anhydride-grafted polypropylene (iPP-*graft*-MA) were selected for reactive compounding. The choice of copolymers was motivated by the fact that p(E-*stat*-GMA) has been used as a reactive compatibiliser for polymer blends[106-108] and for byproduct-free crosslinking of PE-containing blends,[105, 109-112] and because iPP-*graft*-MA possesses good dielectric properties[113, 114] and has been used as a compatibiliser, coupling agent, and interface modifier for PP-based materials.[115, 116]

The reaction between p(E-*stat*-GMA) and iPP-*graft*-MA involves an initial step to activate the succinic anhydride followed by the covalent linking of p(E-*stat*-GMA) with the activated iPP-*graft*-MA (Figure 13). The first step is moisture-initiated, where water opens the succinic acid anhydride ring to form two carboxyl groups. Fourier Transform Infrared (FT-IR) spectroscopy of iPP-*graft*-MA confirms that atmospheric moisture is sufficient for this equilibrium reaction between the anhydride and di-acid to occur, evident in the 1781 cm^{-1} peak for the anhydride and the 1718 cm^{-1} peak for the acid (Figure 14a and 14b).[117] Although higher temperatures favour the closed anhydride form, there is an appreciable amount of the di-acid form at 170 °C that is necessary to melt the iPP crystals in iPP-*graft*-MA (T_m^{PP} ~ 155 °C).

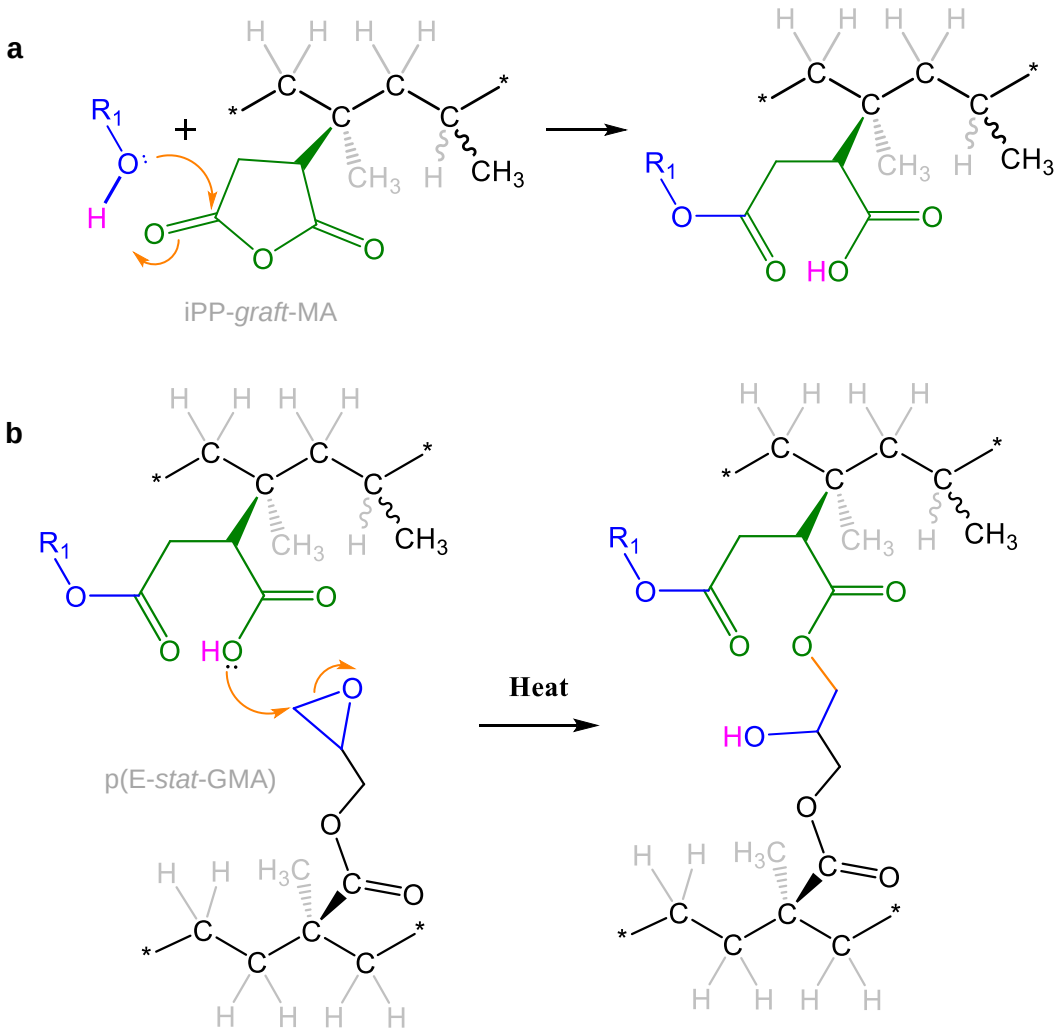

Figure 13. (**a**) Activation of iPP-*graft*-MA by ring opening through reaction with water leading to two carboxyl groups, and (**b**) a carboxylic acid group reacts with an epoxy group, part of the GMA comonomer of p(E-*stat*-GMA); the second carboxyl group carries a generic R_1 group because ring opening can occur by reaction with water (R_1 = H) but also another carboxyl group or a hydroxyl group that is formed through an epoxy ring-opening reaction.

In a second step, the nucleophilic oxygen of the generated carboxyl group attacks the electrophilic carbon of the epoxy ring in p(E-*stat*-GMA). The reaction leads to an ester bond between the two copolymers, without releasing any byproducts. This has also been confirmed by FT-IR analysis of a binary blend comprising p(E-*stat*-GMA) and iPP-*graft*-MA in a ratio of 4:1 by weight, where epoxy and carboxyl groups would be present in a 1:1 molar ratio if all the anhydride rings were open. After annealing the binary blend for 20 minutes at 170 °C, reaction between the two copolymers is evident by the decrease in height of the 1781 cm^{-1} anhydride peak and the increase in intensity of the 1718 cm^{-1} acid peak (Figure 14c).

As the epoxy-acid reaction proceeds between the two copolymers, acid groups are consumed, which shifts the equilibrium towards the opening of more anhydrides. This reduces the number of anhydride rings present and increases the concentration of carboxyl groups, as observed by FT-IR. The reaction between p(E-*stat*-GMA) and iPP-*graft*-MA is further evidenced by the consumption of the epoxy group in the binary blend relative to neat p(E-*stat*-GMA). This is reflected in the reduced intensity of the peak at 911 cm^{-1} (which corresponds to the C-O deformation of the epoxy ring)[118-120] in the binary blend compared to neat p(E-*stat*-GMA) (Figure 14d).

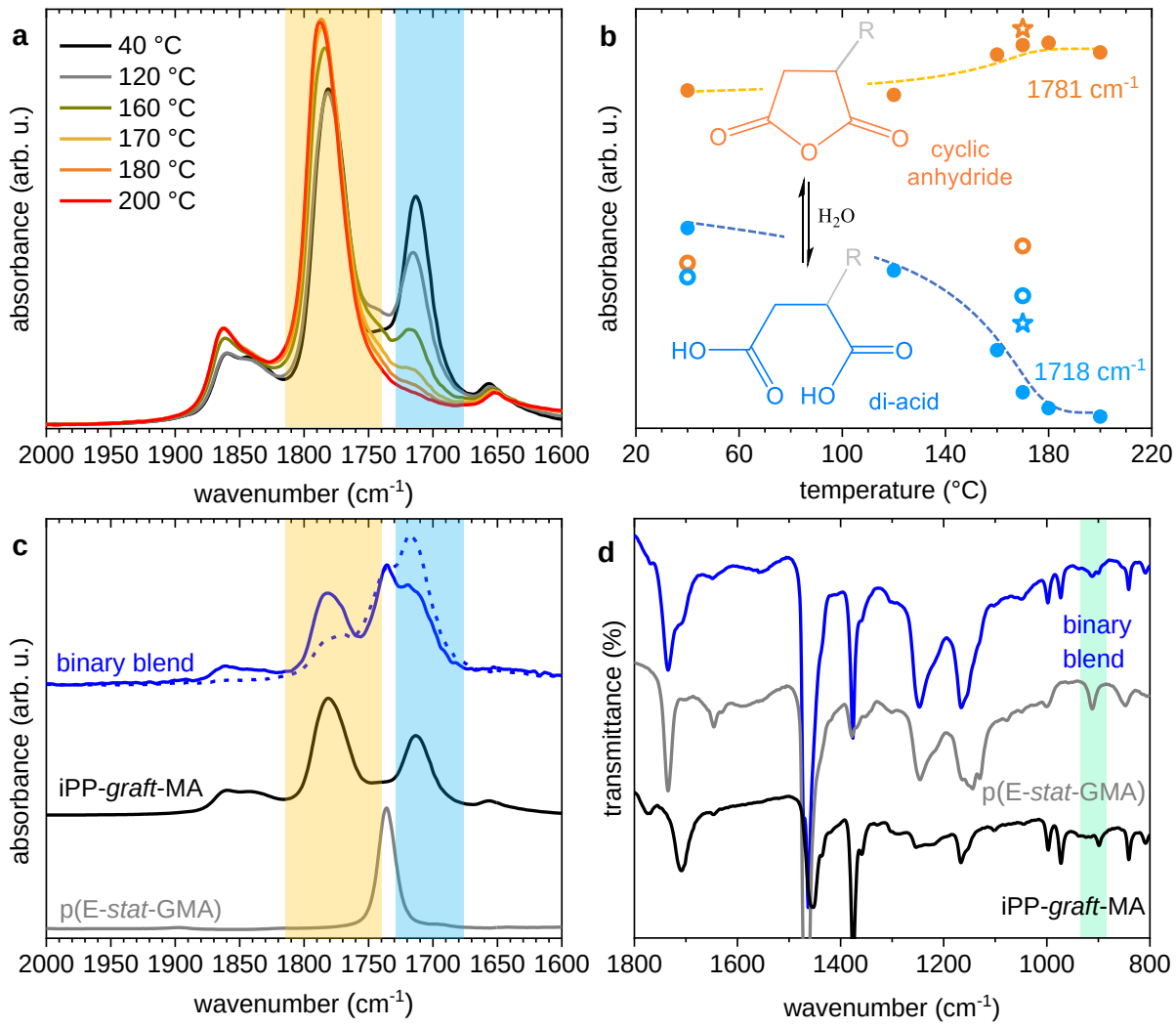

Figure 14. (a) Transmission FT-IR spectra of iPP-*graft*-MA at increasing temperatures from 40 °C to 220 °C, **(b)** absorbance intensity at 1718 cm^{-1} for the acid (blue) and 1781 cm^{-1} for the anhydride (orange) plotted against temperature for iPP-*graft*-MA (filled circles), the binary blend (hollow circles), and the binary blend after 20 minutes at 170 °C (hollow star); inset: reaction scheme of the reversible conversion between the cyclic anhydride and opened di-acid forms of the succinic anhydride grafted onto iPP, where R = iPP chain, **(c)** transmission FT-IR spectra measured near room temperature of p(E-*stat*-GMA) (grey, solid), iPP-*graft*-MA (black, solid), the binary blend compounded for 5 minutes at 170 °C (blue, solid) and the same binary material after annealing at 170 °C for 20 minutes (blue, dashed), and **(d)** ATR FT-IR spectra of the binary blend (blue), p(E-*stat*-GMA) (grey) and iPP-*graft*-MA (black), measured at room temperature.

7.2 The effect of in-situ copolymer formation on thermomechanical properties

The cured binary blend exhibited a rubber plateau that was higher than neat LDPE and comparable to reference XLPE (Figure 15). However, the binary blend is a thermoset (determined by gel content experiments – details in *paper I*), and *E'* remains high even above T_m^{PP} ~ 155 °C. To obtain a thermoplastic blend, a 24:6:70 p(E-*stat*-GMA):iPP-*graft*-MA:LDPE ternary blend, which contains the same ratio of the copolymers as in the binary blend but also a majority phase of 70 wt% LDPE, was prepared. In this ternary blend, the storage modulus above T_m^{LDPE} (and above T_m^{PP}) was substantially reduced compared to the 4:1 p(E-*stat*-GMA):iPP-*graft*-MA binary blend, but still substantially above that of neat LDPE.

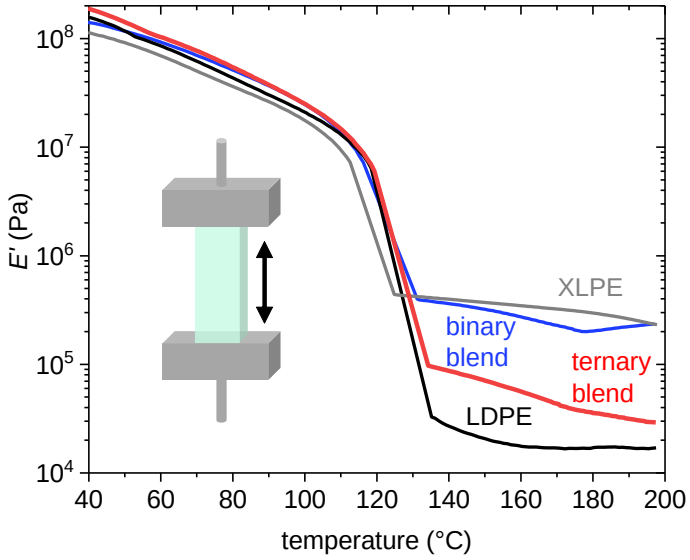

Figure 15. Storage modulus *E'* measured with DMA as a function of temperature of the 4:1 p(E-*stat*-GMA):iPP-*graft*-MA binary blend compounded at 170 °C for 5 minutes (blue), the 24:6:70 p(E-*stat*-GMA):iPP-*graft*-MA:LDPE ternary blend compounded at 170 °C for 10 minutes (red), as well as LDPE (black) and XLPE, i.e. LDPE crosslinked with 1 wt% dicumyl peroxide (DCP) at 200 °C (grey); inset: schematic of the oscillatory DMA measurement indicating the direction of the applied stress.

To assess the ternary blend's ability to resist deformation outside the elastic region at temperatures above T_m^{LDPE}, creep measurements were carried out (Figure 16). When subjected to a constant stress of 1 kPa above T_m^{LDPE} at 120 °C, neat LDPE yielded within 10 minutes. In contrast, the ternary material displayed strongly reduced creep above T_m^{LDPE} at 120 °C and 130 °C, exhibiting creep strain of not more than 30% even after 100 minutes. The creep resistance demonstrated by the ternary blend can be attributed to the reaction between p(E-*stat*-GMA) and iPP-*graft*-MA which not only introduces crosslinks, but also effectively reduces the degree of phase separation in the blend (Figure 17). This allows iPP crystals to provide the thermomechanical reinforcement necessary to resist creep at $T_m^{LDPE} < T < T_m^{PP}$. However, above this temperature window, eg. at 170 °C, this reinforcement is lost and the ternary blend displays a high creep strain approaching 120 % after 100 minutes. This suggests that the ternary blend can be reprocessed and was confirmed when the re-extruded ternary blend maintained a creep strain below 30 % after 100 minutes at 120 °C. The creep resistance demonstrated by the ternary blend even after re-extrusion reflects the material's potential for recyclability by remelting.

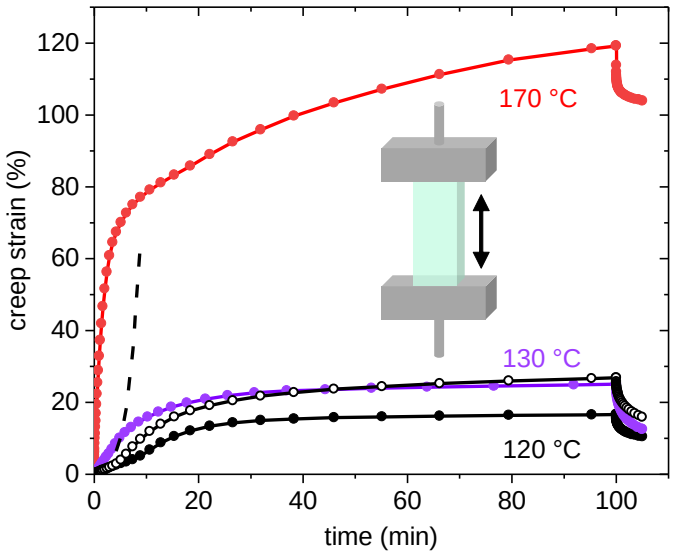

Figure 16. Creep strain at a constant stress of 1 kPa (equivalent to the sample weight) at 120 °C (black), 130 °C (purple) and 170 °C (red), of the 24:6:70 p(E-*stat*-GMA):iPP-*graft*-MA:LDPE ternary blend compounded at 170 °C for 10 minutes (filled circles), and at 120 °C for the ternary blend after a second compounding step at 170 °C for 5 minutes (black, hollow circles) and neat LDPE (black, dashed line); inset: schematic of the creep measurement indicating the direction of the applied stress.

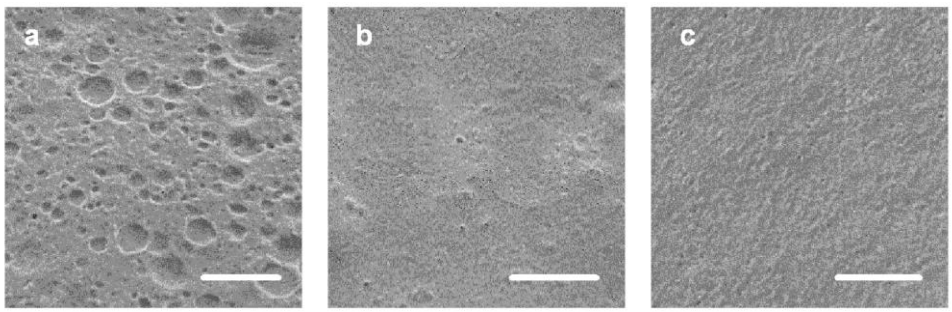

Figure 17. SEM images of cryofractured, etched and sputtered surfaces of **(a)** the 4:1 LDPE:iPP blend, **(b)** the 4:1 p(E-*stat*-GMA):iPP-*graft*-MA binary blend, and **(c)** the 24:6:70 p(E-*stat*-GMA):iPP-*graft*-MA:LDPE ternary blend (scale bar = 5 µm).

7.3 DC electrical conductivity

In terms of electrical properties, the DC electrical conductivity measured at 70 °C and electric field of 30 kV mm^{-1} after 18 h, was σ_{DC} ~ 4·10^{-14} S m^{-1} for the ternary blend (Table 1), comparable to σ_{DC} of XLPE despite the presence of polar groups in the copolymers.

material	σ_{DC} after 18 h at 70 °C and 30 kV/mm* (10^{-14} S m^{-1})
LDPE	3 (± 0.3)
XLPE	4 (± 0.4)
ternary blend	4 (± 0.4)

Table 1. DC electrical conductivity at 70 °C and an electric field of 30 kV mm^{-1} after 18 h, σ_{DC}, of LDPE, XLPE, the 4:1 p(E-*stat*-GMA):iPP-*graft*-MA binary blend and the 24:6:70 p(E-*stat*-GMA):iPP-*graft*-MA:LDPE ternary blend compounded at 170 °C; error of σ_{DC} are based on values measured for three neat LDPE samples. *DC electrical conductivity measurements were done by Amir Masoud Pourrahimi (Chalmers)*

7.4 Challenges

While the behaviour of the here described ternary blend is promising, the reaction mechanism used for in-situ copolymer formation involves water. Changes in atmospheric humidity with the seasons can affect the reproducibility of the ternary blend's thermomechanical performance. This can be remedied by adding water to the system, but a better solution would be a humidity control chamber, which would allow to control the equilibrium of the reaction mechanism involved and hence material properties. However, reaction mechanisms that are less reversible and do not involve moisture are more practical. These will elevate the potential of reactive compounding of LDPE and iPP as a means of preparing thermoplastic insulation materials for high voltage cable insulation.

Chapter 8

Ternary Blends Comprising LDPE, Isotactic PP and a Styrenic Copolymer

The properties of blends can be affected by a wide range of factors, including blend composition, compounding temperature, compounding time, mixing speed and processing conditions after compounding. With the complexities associated with compounding, the blending of unfunctionalised polyolefins reduces the number of factors to consider by eliminating variables associated with the chemical reaction mechanisms involved in reactive compounding. In this chapter, the properties of iPP:LDPE blends processed under comparable conditions but with different compositions are studied to investigate how the addition of styrenic block copolymers affects the properties of these blends.

8.1 Screening styrenic block copolymers as potential compatibilisers for iPP:LDPE blends

The linear triblock copolymer polystyrene-*b*-poly(ethylene-co-butylene)-*b*-polystyrene (SEBS) is widely used as an impact modifier for PP[121, 122] and as a compatibiliser for various polymer blends, including those of PP and linear polyethylenes like HDPE and LLDPE.[123, 124] However, little research has been done on the compatibilisation of iPP and LDPE with SEBS. Hence, a range of different styrene-based block copolymers (Table 2) were screened for their ability to increase the stiffness at $T_m^{LDPE} < T < T_m^{PP}$ compared to the 25:75 iPP:LDPE binary blend, which features a low E'~ $2 \cdot 10^4$ Pa at 150 °C (Figure 18). 16 styrene-based block copolymers were screened that varied in terms of melt flow index, styrene block length, chemical composition of the middle block (i.e. ethylene-butylene, isoprene, butadiene, or ethylene-propylene, and one grade grafted with maleic anhydride), composition of diblock copolymers, and degree of branching.

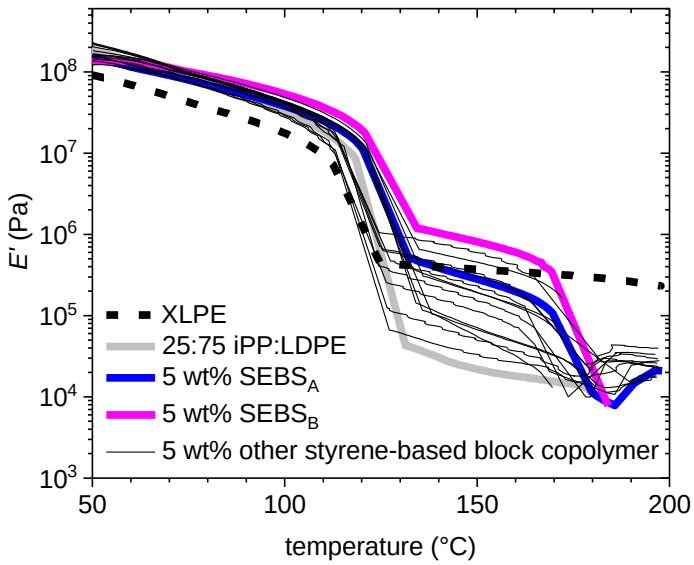

Figure 18. Storage modulus *E'* measured with DMA as a function of temperature of XLPE (black, bold dashed line), 25:75 iPP:LDPE binary blend (grey, bold solid line), and 5:95 additive:(PP:LDPE)$_{25:75}$ ternary blends with 16 different styrene-based block copolymers (black, solid lines) – curves highlighted in colour contain SEBS$_A$ (blue, bold solid line) and SEBS$_B$ (magenta (or violet in print version), bold solid line) as additives.

While it was not possible to establish any correlation between the characteristics of the different copolymers tested and the compatibilisation potential of the copolymers (and microstructure of the blends), it is clear that incorporating these copolymers increased the height of the rubber plateau of the ternary blends compared to the 25:75 iPP:LDPE binary blend, to varying degrees. In this thesis, focus will be placed on blends that incorporate two grades of SEBS – SEBS$_A$ and SEBS$_B$. The ternary blend with SEBS$_A$ features a rubber plateau well above that of the 25:75 iPP:LDPE binary blend, matching that of reference XLPE up to almost 150 °C. This led to initial investigations (*paper II*) on 25:75 iPP:LDPE blends with SEBS$_A$. This was followed by more in-depth studies on blends with SEBS$_B$ (tested at a later stage of the project), since DMA measurements suggest SEBS$_B$ to be the most effective of the screened copolymers at enhancing the stiffness of the 25:75 iPP:LDPE binary blend at $T_m^{LDPE} < T < T_m^{PP}$.

Label	Supplier	Type of copolymer	Styrene content (%)	Melt flow index (g/10 min)	Other comments
G1645MO	KRATON	SEBS	11.5 - 13.5	2 - 4.5 (230 °C, 2.16 kg)	$SEBS_A$
G1642HU	KRATON	SEBS	18.5 - 22.5	<1 (230 °C, 2.16 kg)	$SEBS_B$
A1535HU	KRATON	SEBS	56.3 - 60.3	<1 (230 °C, 5 kg)	-
G1726VS	KRATON	SEBS	30.0 - 32.0	15.0 - 23.0 (190 °C, 2.16 kg)	-
G1640ES	KRATON	SEBS	30.7 - 32.7	not provided	-
MD6684GS	KRATON	SEBS	32.9	20 (230 °C, 2.16 kg)	grafted with 1% maleic anhydride
G1702HU	KRATON	SEPS	26.2 - 29.0	<1 (230 °C, 5 kg)	-
G1730VO	KRATON	SEPS	18.5 - 22.5	11.2 (230 °C, 5 kg)	-
P5051	Tuftec	SEBS	47	4 (190 °C, 2.16 kg)	-
P1083	Tuftec	SEBS	20	3 (190 °C, 2.16 kg)	-
SBS 1	Sigma Aldrich	SBS	28	not provided	-
SBS 2	Sigma Aldrich	SBS	30	not provided	M_w = 140 kg mol^{-1}
SBS 3	Sigma Aldrich	SBS	30	not provided	contains 80% diblock
SBS 4	Sigma Aldrich	SBS	21	not provided	branched
SBS 5	Sigma Aldrich	SBS	30	not provided	branched
SIS	Sigma Aldrich	SIS	22	not provided	-

Table 2. Supplier, styrenic copolymer midblock (ethylene-butylene in SEBS, ethylene-propylene in SEPS, butadiene in SBS, and isoprene in SIS), styrene content and melt flow index of styrenic copolymers tested as compatibilisers for the 25:75 iPP:LDPE binary blend.

8.2 Effect of SEBS on iPP:LDPE blends

8.2.1 Thermomechanical properties

In case of the $SEBS_A$:iPP:LDPE ternary blends, the incorporation of either 5 or 10 wt% of $SEBS_A$ increased *E'* at $T_m^{LDPE} < T < T_m^{PP}$ to a similar extent relative to the 25:75 iPP:LDPE binary blend (Figure 19a). In addition to the heightened *E'* in this temperature window measured by DMA in tensile mode, the 10:90 $SEBS_A$:$(iPP:LDPE)_{25:75}$ ternary blend also demonstrated improved resistance to deformation under compressional stress (measured with the TMA) relative to the binary blend when heated above T_m^{LDPE} (Figure 19c). This is reflected in the reduced penetration depth of the measurement probe in case of the ternary blend as compared to the binary blend at 110 °C $< T <$ 150 °C.

Apart from DMA experiments, the $SEBS_A$:$(iPP:LDPE)_{25:75}$ ternary blend was also subjected to a constant stress at elevated temperatures where the deformation of the material was measured as a function of time. At 130 °C, this ternary blend demonstrated significantly less deformation than the binary blend in these creep tests, both when subjected to tensile stress (Figure 19b) and when subjected to compressional stress (Figure 19d). The creep strain of 6% demonstrated by the ternary blend after 100 minutes in the tensile creep experiment was comparable to the creep strain of 4% exhibited by XLPE. In the compressional creep experiment, the ternary blend displayed greater resistance to deformation than XLPE.

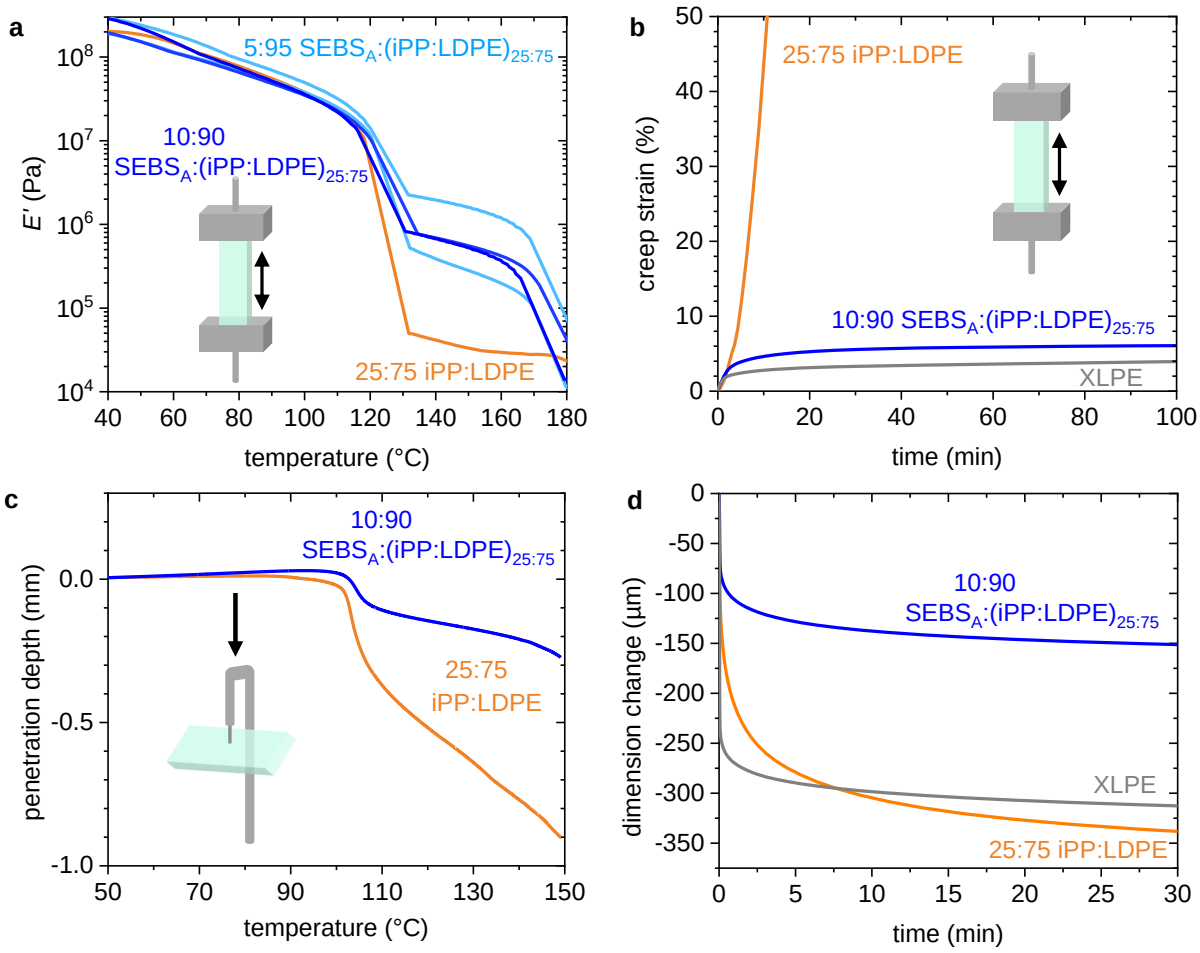

Figure 19. (a) Storage modulus *E'* from DMA of the 25:75 iPP:LDPE binary blend (orange), and ternary blends 5:95 SEBS$_A$:(iPP:LDPE)$_{25:75}$ (sky blue) and 10:90 SEBS$_A$:(iPP:LDPE)$_{25:75}$ (blue); **(b)** creep strain at a constant stress of 1 kPa (equivalent to the sample weight) of the binary blend (orange), the 10:90 SEBS$_A$:(iPP:LDPE)$_{25:75}$ ternary blend (blue) and XLPE (grey) at 130 °C as a function of time; **(c)** penetration depth measured as a function of temperature from indentation measurements of anisotropic samples of the 25:75 iPP:LDPE binary (orange) and the 10:90 SEBS$_A$:(iPP:LDPE)$_{25:75}$ ternary blend (blue); and **(d)** indentation creep strain of the 25:75 iPP:LDPE binary blend (orange), the 10:90 SEBS$_A$:(iPP:LDPE)$_{25:75}$ ternary blend (blue) and XLPE (grey) at 130 °C and under 10 kPa stress, as a function of time.

The promising thermomechanical properties demonstrated by the 10:90 $SEBS_A$:(iPP:LDPE)$_{25:75}$ ternary blend led to further investigations on SEBS:iPP:LDPE systems using $SEBS_B$, which gave rise to ternary blends with an even higher stiffness than the $SEBS_A$-based blends.. $SEBS_B$, iPP, LDPE and their blends, which spanned a wide range of compositions, were characterised to better understand the SEBS:iPP:LDPE system.

Since the interactions among the different polymers in a blend can influence material properties, binary blends of iPP:LDPE, iPP:$SEBS_B$ and LDPE:$SEBS_B$ were first characterised with DSC. T_m^{LDPE} and T_m^{PP} of iPP:LDPE blends, and T_m^{PP} of iPP:$SEBS_B$ binary blends obtained from first heating DSC thermograms, were observed to remain fairly constant as a function of iPP content (Figure 20). The endothermic peaks corresponding to T_g^{PS} in $SEBS_B$ and/or T_m^{LDPE} in LDPE:$SEBS_B$ binary blends also showed little change with blend composition. These observations reflect the immiscible nature of the three polymers.

SEM micrographs were also taken of cryofractured, etched and sputtered samples of the binary blends 20:80 iPP:LDPE, 20:80 $SEBS_B$:LDPE, 20:80 $SEBS_B$:iPP and 80:20 $SEBS_B$:iPP (Figure 21). For the $SEBS_B$-containing samples (Figures 21b-d), the dark regions correspond to $SEBS_B$ since it is amorphous as has been shown in wide-angle X-ray scattering (WAXS) measurements (Figure 22) and is therefore removed during the etching process prior to imaging. These SEM micrographs show that LDPE, iPP and $SEBS_B$ strongly phase separate in the binary blends. Interestingly, in contrast to the large domains in the 20:80 iPP:LDPE and 20:80 $SEBS_B$:LDPE binary blends, much smaller domains are observed in the 20:80 $SEBS_B$:iPP and 80:20 $SEBS_B$:iPP blends. This suggests better compatibility between $SEBS_B$ and iPP compared to the other polymer pairs.

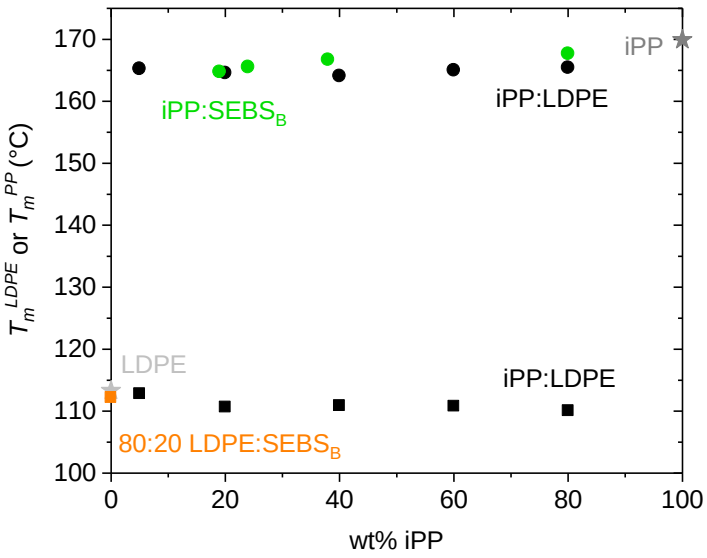

Figure 20. Peak melting temperature of iPP T_m^{PP} as a function of iPP content (wt%) for the iPP:SEBS$_B$ (green circles) and iPP:LDPE (black circles) binary blends, and neat iPP (dark grey star); and the peak melting temperature of LDPE T_m^{LDPE} of iPP:LDPE binary blends (black squares), neat LDPE (light grey star), and the 80:20 LDPE:SEBS$_B$ binary blend (orange square), based on first heating DSC thermograms.

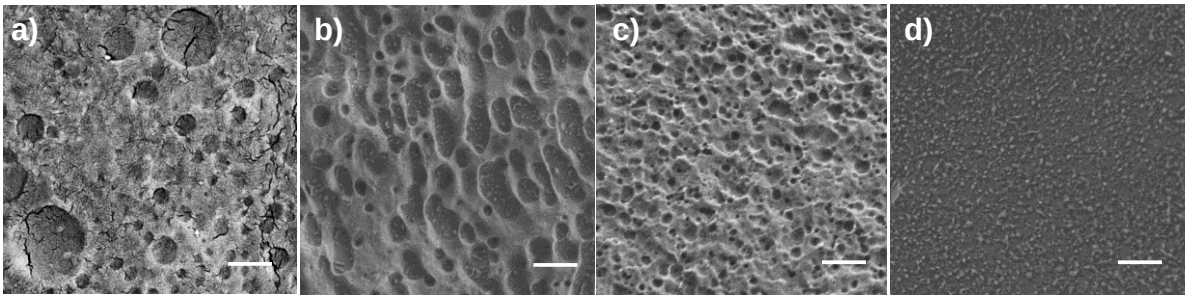

Figure 21. SEM images of cryofractured, etched and sputtered surfaces of the binary blends **(a)** 20:80 iPP:LDPE, **(b)** 20:80 SEBS$_B$:LDPE, **(c)** 20:80 SEBS$_B$:iPP and **(d)** 80:20 SEBS$_B$:iPP (scale bar = 2 µm).

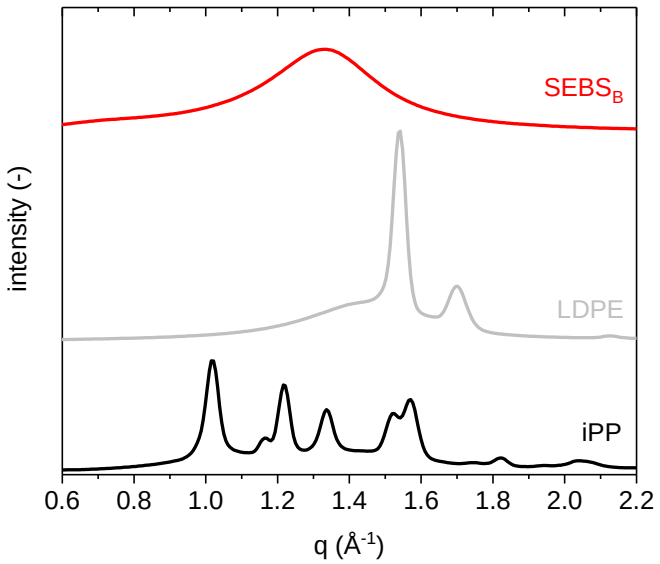

Figure 22. WAXS diffractograms of neat iPP (black), neat LDPE (grey), and neat SEBS$_B$ (red), where the broad peak featured in SEBS$_B$ reflects the amorphous nature of SEBS$_B$. *WAXS measurements were done by Anja Lund and Ida Östergren (Chalmers)*

The varying degrees of compatibility among SEBS$_B$, iPP and LDPE influence the microstructures of the SEBS$_B$:iPP:LDPE ternary blends. 5:95 SEBS$_B$:(iPP:LDPE) ternary blends with iPP:LDPE ratios of 20:80, 25:75, 40:60 and 60:40 feature two main regions – one comprising neat LDPE and another comprising both iPP and SEBS$_B$ (Figure 23). In these blends, SEBS$_B$ assembles within the iPP-SEBS$_B$ regions as small sub-domains (which is etched out, leaving dark 'holes'), and sometimes at the interface between iPP and LDPE (*see paper II*). The resulting salami-like microstructure can be attributed to the preferential interaction between iPP and SEBS$_B$ since they have better compatibility compared to the other polymer pairs in the ternary blend. However, there are no significant changes between the binary and ternary blends (at each iPP:LDPE composition ratio with constant SEBS$_B$ content of 5 wt%) in terms of domain sizes and the distribution of the domains that would be expected from a conventional compatibiliser (Figure 23).

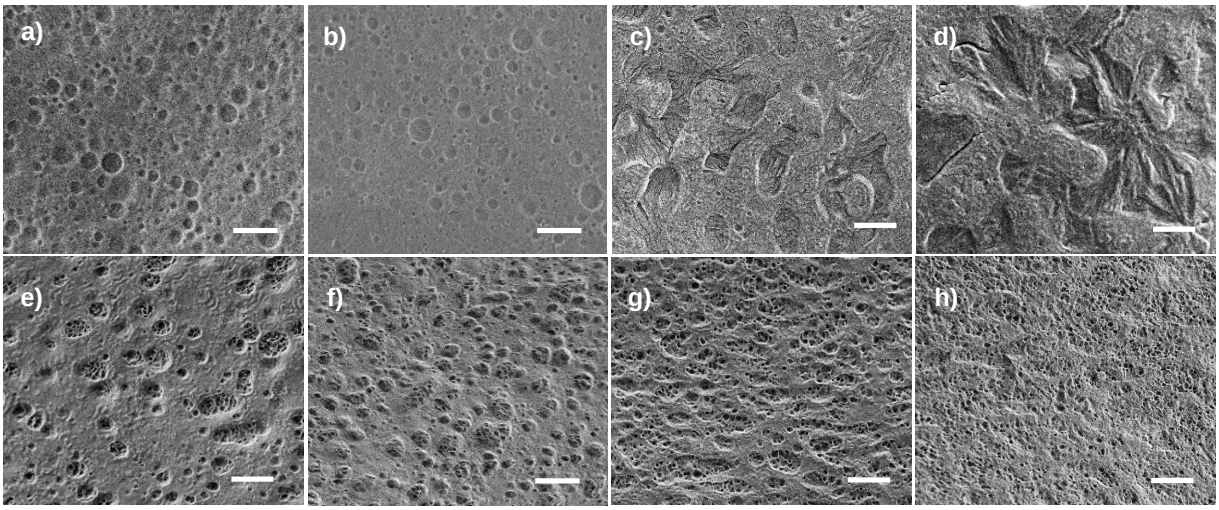

Figure 23. SEM images of cryofractured, etched and sputtered surfaces of iPP:LDPE binary blends with iPP:LDPE ratios of: **(a)** 20:80, **(b)** 25:75 **(c)** 40:60 and **(d)** 60:40, and the 5:95 $SEBS_B$:(iPP:LDPE) ternary blends with iPP:LDPE ratios of: **(e)** 20:80, **(f)** 25:75 **(g)** 40:60 and **(h)** 60:40 (scale bar = 5 μm).

Nevertheless, DMA measurements of neat LDPE, neat iPP, iPP:LDPE binary blends, and 5:95 $SEBS_B$:(iPP:LDPE) ternary blends reveal that the incorporation of 5 wt% $SEBS_B$ lowers the iPP content required to significantly increase *E'* at 150 °C (compared to neat LDPE) from 40 wt% to 24 wt% (Figure 24). This widens the range of compositions at which the 5:95 $SEBS_B$:(iPP:LDPE) ternary blends exhibit an increase in *E'* at 150 °C. This is despite the slight lowering of *E'* at 150 °C for ternary blends with high iPP content (at least 40 wt% iPP) in the presence of $SEBS_B$ since these blends feature continuous iPP or iPP:$SEBS_B$ regions (Figure 23).

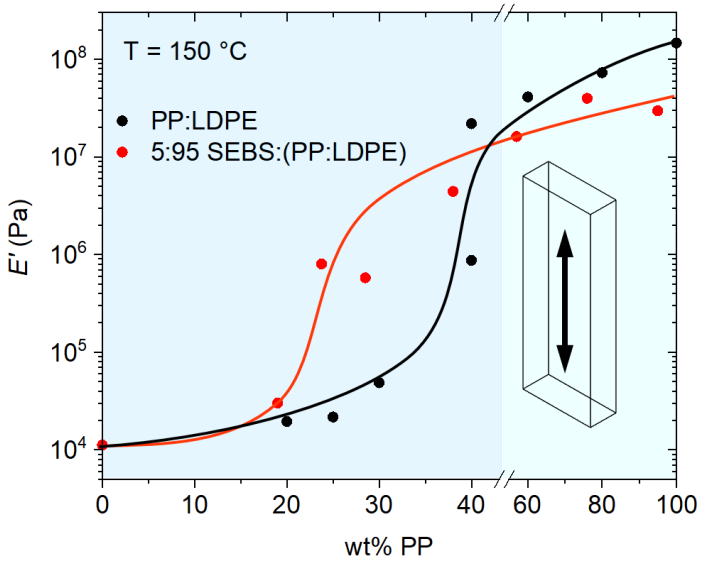

Figure 24. Storage modulus *E'* measured at 150 °C with DMA as a function of iPP content of LDPE, iPP, iPP:LDPE binary blends (black circles), and the corresponding materials with 5 wt% SEBS (red circles); solid lines are a guide to the eye.

To further understand how $SEBS_B$ affects the thermomechanical properties of the $SEBS_B$:iPP:LDPE ternary blends, more SEM and DMA measurements were conducted. Here, the iPP content of the ternary blends was kept constant while the $SEBS_B$ content was varied. SEM images of 24:76 iPP:($SEBS_B$:LDPE) ternary blends show that increasing the $SEBS_B$ content from 5 wt% to 30 wt% (while keeping the iPP content constant at 24 wt%) resulted in coalescence and increasing volume of the iPP:$SEBS_B$ regions (Figure 25). This can be expected since $SEBS_B$ forms coalesced domains in the 20:80 $SEBS_B$:LDPE binary blend, and the volume fraction of LDPE decreases as $SEBS_B$ content increases in the $SEBS_B$:iPP:LDPE ternary blends when the iPP content is kept constant.

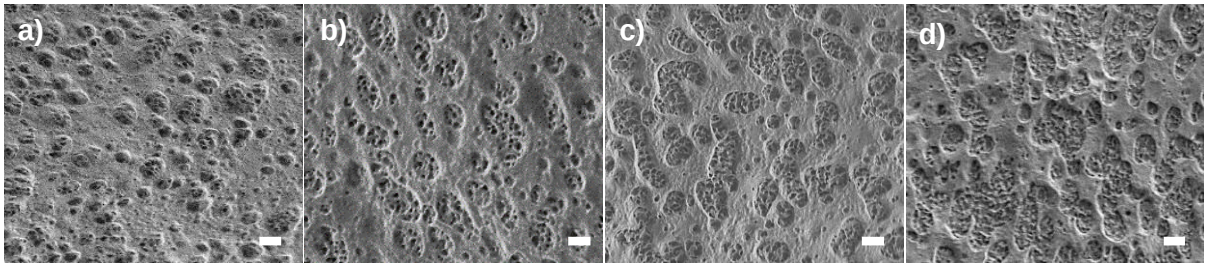

Figure 25. SEM images of cryofractured, etched and sputtered surfaces of 24:76 iPP:(SEBS$_B$:LDPE) ternary blends with SEBS$_B$ content: **(a)** 5 wt%, **(b)** 10 wt% **(c)** 20 wt% and **(d)** 30 wt% (scale bar = 2 μm).

DMA thermograms show that increasing the SEBS$_B$ content in 24:76 iPP:(SEBS$_B$:LDPE) ternary blends heightens *E'* at $T_m^{LDPE} < T < T_m^{PP}$ (Figure 26). Although an increase in SEBS$_B$ content (and a corresponding decrease in LDPE content) results in a greater volume fraction of the iPP:SEBS$_B$ region, the 24:76 iPP:(SEBS$_B$:LDPE) ternary blends containing up to 30 wt% SEBS$_B$ do not show continuity of the iPP:SEBS$_B$ regions (cf. iPP:LDPE binary blends where a heightened rubber modulus was only observed at the onset of continuity of the iPP phase). Yet, these blends still featured an increased stiffness at $T_m^{LDPE} < T < T_m^{PP}$ as the SEBS$_B$ content was increased from 0 wt% to 30 wt%.

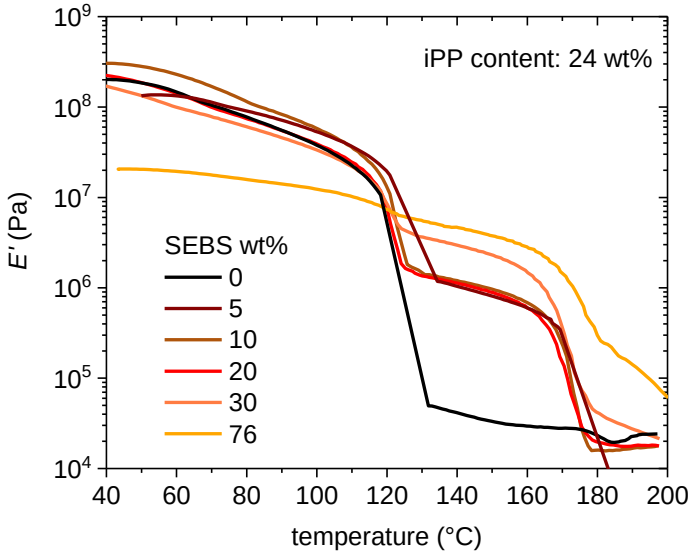

Figure 26. Storage modulus *E'* as a function of temperature from DMA of the 25:75 iPP:LDPE binary blend (black), the ternary blends 24:76 iPP:(SEBS$_B$:LDPE) (different shades of red/orange) and the 24:76 SEBS$_B$:LDPE binary blend (yellow).

To further investigate how SEBS$_B$ increases *E'* of SEBS$_B$:iPP:LDPE ternary blends at $T_m^{LDPE} < T < T_m^{PP}$, DMA thermograms of iPP:SEBS$_B$ and LDPE:SEBS$_B$ binary blends with increasing amounts of SEBS$_B$ were obtained (Figure 27). iPP:SEBS$_B$ binary blends feature an increase in *E'* at temperatures even above T_m^{PP} as the amount of SEBS$_B$ increases (Figure 27a). This is in contrast to neat iPP which features a drastic drop in *E'* upon reaching T_m^{PP} that resulted in the sample yielding at ~180 °C, suggesting that SEBS$_B$ provides some degree of added stiffness above T_m^{PP} in SEBS$_B$ -containing blends.

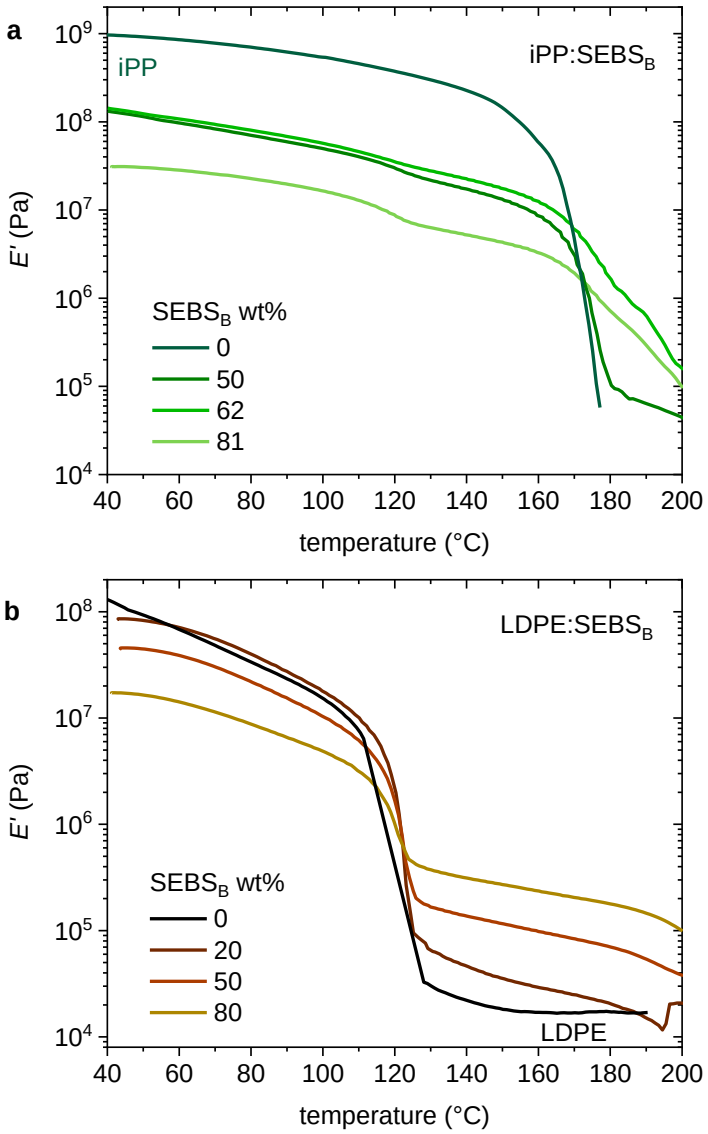

Figure 27. Storage modulus *E'* as a function of temperature from DMA of **(a)** neat iPP (darkest green) and iPP:SEBS$_B$ binary blends of varying compositions (shades of green), and **(b)** neat LDPE (black) and LDPE:SEBS$_B$ binary blends of varying compositions (shades of brown).

**SEBS$_B$ not measured due to difficulty with compounding of neat SEBS$_B$. Refer to supporting information in paper III for shear storage modulus G' of SEBS$_B$ measured as a function of temperature, measured by oscillatory shear rheology.*

The enhanced high temperature stiffness provided by $SEBS_B$ is also observed in LDPE:$SEBS_B$ binary blends (Figure 27b). By incorporating 80 wt% $SEBS_B$, *E'* at 120 - 200 °C of the 20:80 LDPE:$SEBS_B$ binary blend greatly increased relative to neat LDPE. This binary blend featured $E' \sim 3 \cdot 10^5$ Pa and $1 \cdot 10^5$ Pa at 150 °C and 200 °C respectively, which is about one order of magnitude above *E'* of LDPE at these temperatures. To rule out chemical crosslinking due to degradation of the polymers, oscillatory shear rheometry of neat LDPE, iPP and $SEBS_B$ was carried out at the compounding temperature of 180 °C, which showed no change in shear storage modulus *G'* for 30 minutes (Figure 28). Although the stiffness-enhancing effect of $SEBS_B$ above T_m^{LDPE} is not yet fully understood, it is clear that the iPP dispersion in $SEBS_B$:iPP:LDPE ternary blends cannot be the sole consideration when rationalising the heightened *E'* at $T_m^{LDPE} < T < T_m^{PP}$ for $SEBS_B$:iPP:LDPE ternary blends (below the percolation threshold of the iPP-$SEBS_B$ regions) relative to the corresponding iPP:LDPE binary blends.

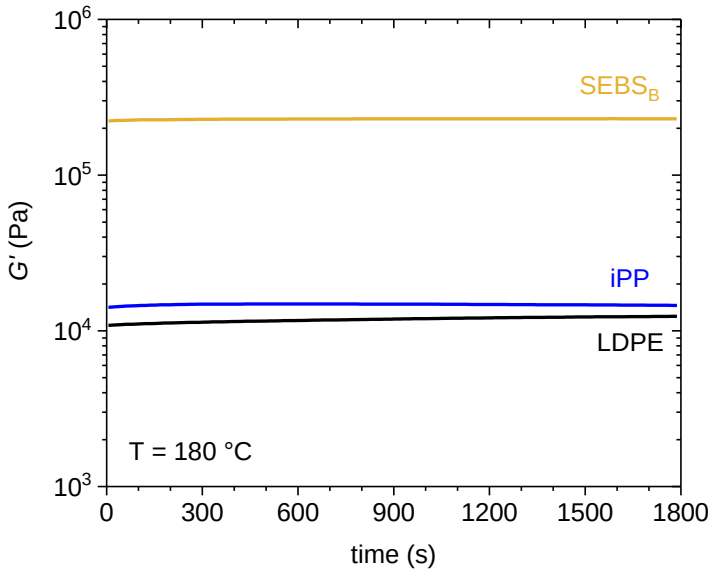

Figure 28. Storage modulus *G'* measured by shear rheometry at 180 °C as a function of time of neat LDPE (black), neat iPP (blue) and neat $SEBS_B$ (yellow).

In addition to increased *E'* above T_m^{LDPE} for SEBS$_B$:iPP:LDPE blends below the percolation threshold of the iPP-SEBS$_B$ regions, incorporating SEBS$_B$ also lowers *E'* below T_m^{LDPE} in these blends compared to the corresponding blends without SEBS$_B$ (Figures 26, 27, 29). This lowering of *E'* below T_m^{LDPE} is important for blends with high iPP content because excessive stiffness at low temperatures is undesirable for cable applications. The effect of SEBS$_B$ on the stiffness of SEBS$_B$:iPP:LDPE ternary blends, also visualised in contour plots of *E'* at 150 °C and 50 °C for the SEBS$_B$:iPP:LDPE ternary system (Figure 29), widens the range of compositions at which the blends demonstrate both enhanced stiffness at $T_m^{LDPE} < T < T_m^{PP}$ and enhanced flexibility at lower temperatures. This may facilitate the tailoring of such materials for use as HVDC cable insulation (Chapter 3).

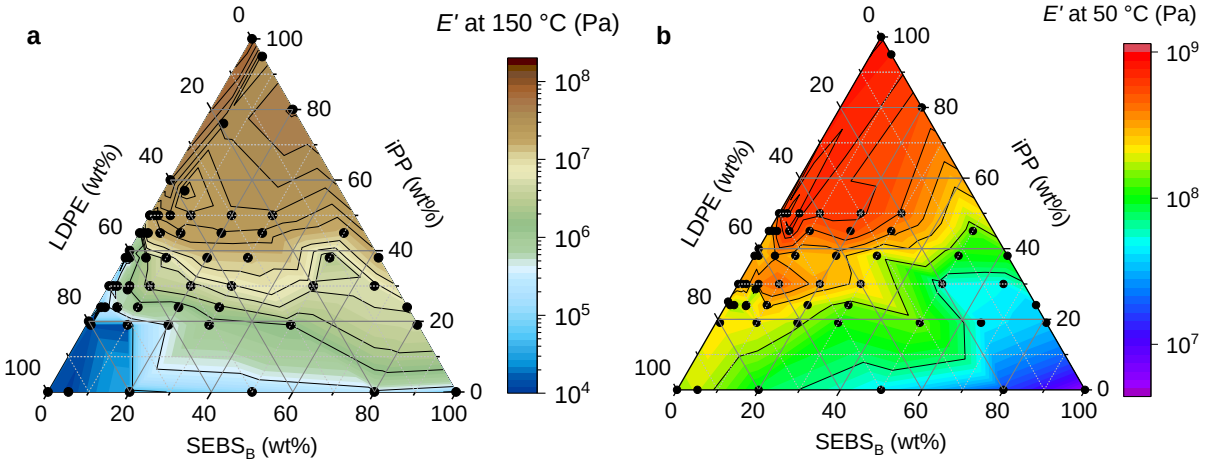

Figure 29. Ternary contour plots showing the storage moduli *E*' of the SEBS$_B$:iPP:LDPE ternary system at **(a)** 150 °C and **(b)** 50 °C.

Another advantage of adding SEBS$_B$ to iPP:LDPE blends is increased robustness against slight changes in processing conditions. This was observed in case of the 5:95 SEBS$_B$:(iPP:LDPE)$_{40:60}$ ternary blend, which showed significantly less variation in *E*' at 150 °C than the 40:60 iPP:LDPE binary blend when subjected to different compounding times of 5 to 15 minutes (Figure 30a). A feasible explanation for this could be microstructure stabilisation in the presence of SEBS$_B$ in the SEBS$_B$:(iPP:LDPE)$_{40:60}$ ternary blend (Figure 30b).

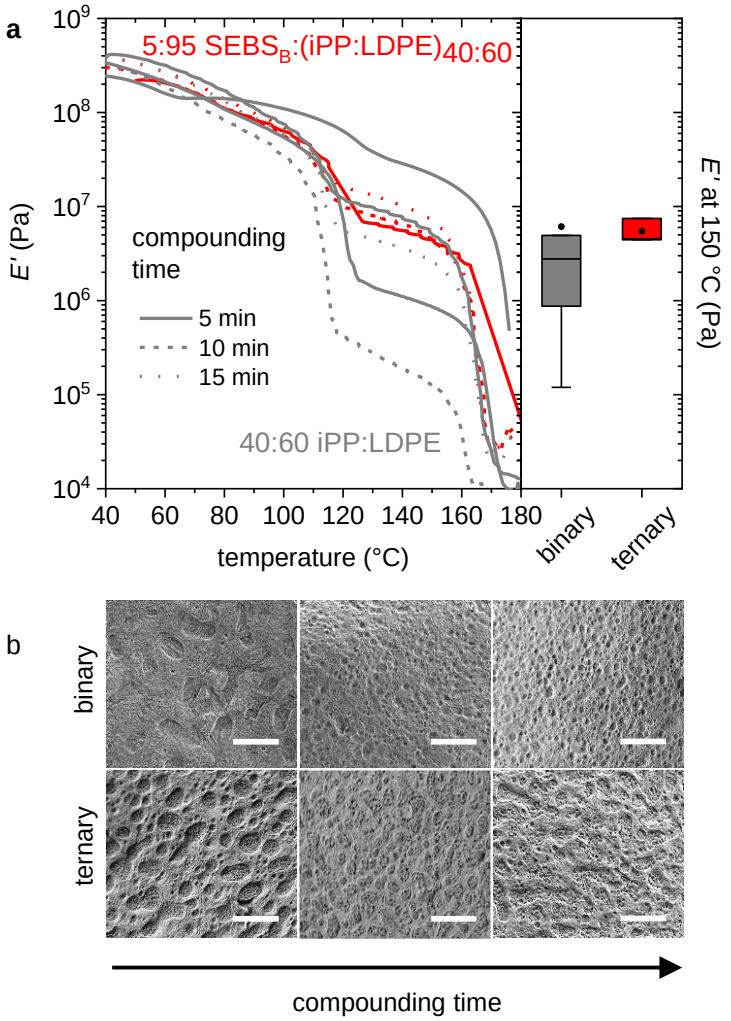

Figure 30. (a) Left: Storage modulus *E*' measured with DMA as a function of temperature of the 40:60 iPP:LDPE binary blends (grey) and the corresponding 5:95 SEBS$_B$:(iPP:LDPE)$_{40:60}$ ternary blends (red). Solid, dashed and dotted lines correspond to compounding times of 5, 10, and 15 minutes respectively; right: box plots of *E*' at 150 °C of the 40:60 iPP:LDPE binary blends (grey) and the corresponding 5:95 SEBS$_B$:(iPP:LDPE)$_{40:60}$ ternary blends (red) at different compounding times, where the box corresponds to the interquartile range, the line in each box reflects the median, the filled circle represents the mean, and the whiskers show the 1.5 interquartile range (right); **(b)** SEM micrographs of the cryofractured, etched and sputtered surfaces of 40:60 iPP:LDPE binary blend (top) and the 5:95 SEBS$_B$:(iPP:LDPE)$_{40:60}$ ternary blend (bottom) after compounding for 5, 10 and 15 minutes (scale bar = 10 µm).

8.2.2 DC electrical conductivity

The neat iPP grade used in this thesis features a low DC electrical conductivity σ_{DC} ~ $1 \cdot 10^{-15}$ S m^{-1} measured at 70 °C and 30 kV mm^{-1} (Figure 31a). The presence of iPP reduces σ_{DC} relative to neat LDPE in case of the iPP:LDPE binary blends and the 5:95 SEBS$_B$:(iPP:LDPE) ternary blends. In fact, incorporating as little as 10 wt% iPP greatly suppressed σ_{DC} from $3 \cdot 10^{-14}$ S m^{-1} for neat LDPE to σ_{DC} ~ $4 \cdot 10^{-15}$ S m^{-1} for the 10:90 iPP:LDPE binary blend. Increasing iPP content beyond 10 wt% further reduced σ_{DC}, but to a lesser degree than the drop in σ_{DC} exhibited by the 10:90 iPP:LDPE binary blend compared to neat LDPE.

In terms of how SEBS$_B$ affects σ_{DC}, a comparison between σ_{DC} of the iPP:LDPE binary blends and the 5:95 SEBS$_B$:(iPP:LDPE) ternary blends shows little influence of 5 wt% SEBS$_B$ on σ_{DC}. The DC electrical conductivity measured for neat SEBS$_B$ σ_{DC} ~ $1 \cdot 10^{-14}$ S m^{-1}, which is slightly lower than σ_{DC} ~ $3 \cdot 10^{-14}$ S m^{-1} for neat LDPE, also suggests that adding SEBS$_B$ should at the very least not be detrimental to the σ_{DC} of the SEBS$_B$:(iPP:LDPE) ternary blends.

8.2.3 Thermal conductivity

The thermal conductivity κ at 70 °C of the iPP:LDPE binary blends and the 5:95 SEBS$_B$:(iPP:LDPE) ternary blends decreases with increasing iPP content (Figure 31b). This is due to the relatively low κ ~ 0.26 W m^{-1}K^{-1} measured for neat iPP compared to neat LDPE, which exhibits a κ ~ 0.36 W m^{-1} K^{-1}. Although neat SEBS$_B$ displays a substantially lower κ ~ 0.19 W m^{-1} K^{-1}, data from the 5:95 SEBS$_B$:(iPP:LDPE) ternary blends and the 30:70 SEBS$_B$:(iPP:LDPE)$_{54:46}$ ternary blend suggest that sufficiently high thermal conductivity values can still be maintained in SEBS$_B$:(iPP:LDPE) ternary blends when the amount of SEBS$_B$ is sufficiently low, preferably less than 30 wt%. These measurements indicate that from a thermal conductivity perspective, SEBS$_B$:(iPP:LDPE) blends that incorporate less iPP and SEBS$_B$ will be more suitable for high voltage cable insulation applications (Chapter 3).

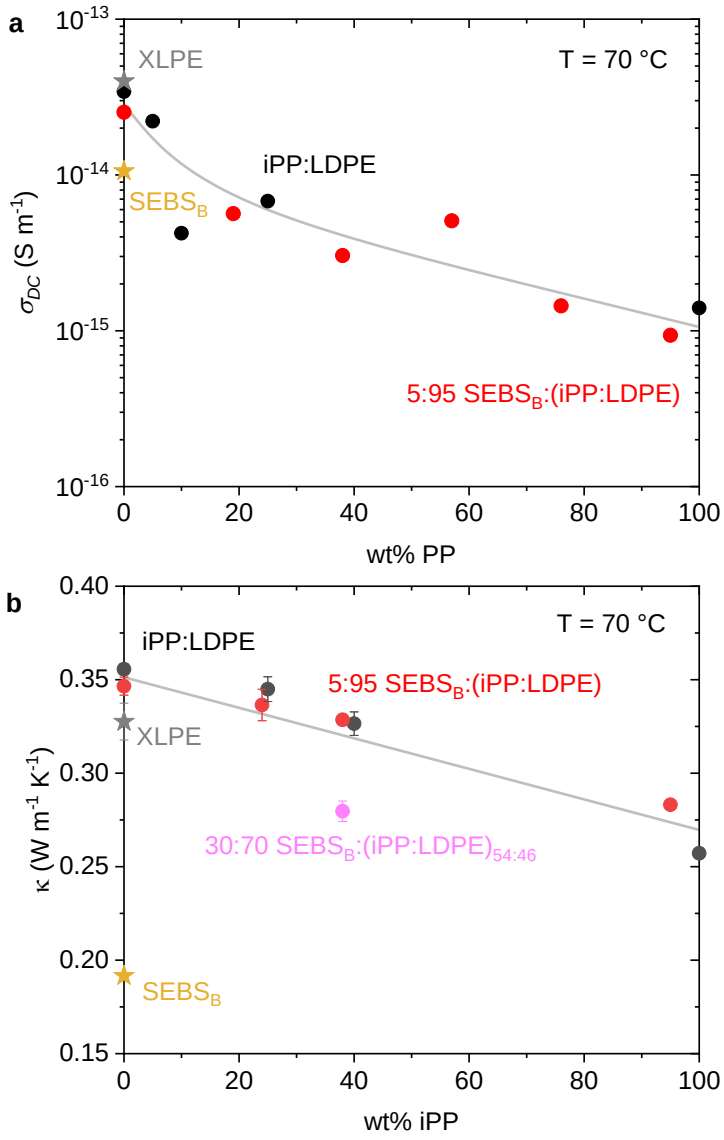

Figure 31. (a) DC electrical conductivity σ_{DC} at 70 °C and 30 kV mm^{-1}, and **(b)** thermal conductivity κ at 70 °C, plotted as a function of iPP content of LDPE, iPP, iPP:LDPE binary blends (black), 5:95 SEBS$_B$:(iPP:LDPE) ternary blends (red), SEBS$_B$ (yellow star), XLPE (grey star) and the 30:70 SEBS$_B$:(iPP:LDPE)$_{54:46}$ ternary blend (pink (or violet in print version), figure 31b only). 10% error is estimated for σ_{DC} based on measurements of three LDPE samples; error bars for κ correspond to the standard deviation from 5 measurements per sample; a solid line is added to each figure to guide the eye. *DC electrical conductivity measurements were done by Amir Masoud Pourrahimi (Chalmers)*

Chapter 9

Reducing DC Electrical Conductivity with Metal Oxide Nanoparticles

$SEBS_B$:iPP:LDPE ternary blends containing Al_2O_3 nanoparticles surface-modified with n-octyltriethoxysilane were studied to investigate the effectiveness of these nanoparticles in reducing the DC electrical conductivity of $SEBS_B$:iPP:LDPE ternary blends. The nanocomposites in this study were prepared using a masterbatch of LDPE with 3 wt% of the surface-modified Al_2O_3 nanoparticles provided by Fritjof Nilsson, KTH (see experimental details in *paper IV*).

The ternary blend with a composition of 20:38:42 $SEBS_B$:iPP:LDPE was selected for this study because it features continuous iPP:$SEBS_B$ regions (Figure 33b) and exhibits a high $E' \sim 15 \cdot 10^6$ Pa at 150 °C that is well above that of XLPE ($E' \sim 0.4 \cdot 10^6$ Pa at 150 °C). This blend also displays $E' \sim 33 \cdot 10^7$ at 50 °C (Table 3), and hence, is substantially less stiff (at lower temperatures like 50 °C) than iPP ($E' \sim 92 \cdot 10^7$ Pa at 50 °C) and similar to the thermoplastic reference hPP ($E' \sim 24 \cdot 10^7$ at 50 °C) (Figure 9). The incorporation of 1.3 wt% Al_2O_3 nanoparticles, which reside primarily in the LDPE phase (Figure 33), had a negligible effect on the blend stiffness, displaying $E' \sim 19 \cdot 10^6$ Pa at 150 °C and $E' \sim 34 \cdot 10^7$ at 50 °C (Table 3).

A σ_{DC}-reducing effect by the Al_2O_3 nanoparticles was observed in both LDPE and the $SEBS_B$:iPP:LDPE ternary blend (Table 3). After 18 h at 70 °C and 30 kV mm^{-1}, the LDPE nanocomposite yielded $\sigma_{DC} \sim 11 \cdot 10^{-15}$ S m^{-1}, which is about a four-fold reduction from $\sigma_{DC} \sim 43 \cdot 10^{-15}$ S m^{-1} of neat LDPE. For the ternary blend, σ_{DC} was slightly reduced from $4.3 \cdot 10^{-15}$ S m^{-1} in the ternary blend to $2.9 \cdot 10^{-15}$ S m^{-1} for the ternary blend nanocomposite. This σ_{DC}-reduction is less prominent compared to that observed in the LDPE nanocomposite because it contains a relatively high amount of the highly insulating iPP. Both iPP and the Al_2O_3

nanoparticles reduce σ_{DC} of LDPE, and are able to do so in a synergistic manner, evidenced by the fact that the ternary blend nanocomposite showed the lowest σ_{DC} compared to the LDPE nanocomposite (iPP absent) and the ternary blend (Al_2O_3 nanoparticles absent).

	$SEBS_B$ (wt%)	iPP (wt%)	LDPE (wt%)	Al_2O_3 (wt%)	E' at 50 °C (10^7 MPa)	E' at 150 °C (10^6 Pa)	σ_{DC} (10^{-15} S m^{-1})
LDPE	-	-	100	-	20	n.a.	43 (± 4.3)
LDPE nanocomposite	-	-	98.7	1.3	21	n.a.	11 (± 0.1)
iPP	-	100	-	-	92	220	1 (± 0.1)
$SEBS_B$	100	-	-	-	0.5	2[a]	10 (± 1)
Ternary blend	20	38	42	-	33	15	4 (± 0.4)
Ternary nanocomposite	20	38	40.7	1.3	34	19	3 (± 0.3)
XLPE	-	-	100	-	9	0.4	40 (± 4)

Table 3. Composition of the investigated formulations, their E' at 50 °C and 150 °C, and σ_{DC} measured at 70 °C and 30 kV mm^{-1} after 18 h. Error in σ_{DC} is estimated to be 10%, based on a comparison of three neat LDPE samples. *σ_{DC} and E'were measured by Azadeh Soroudi (Chalmers)*

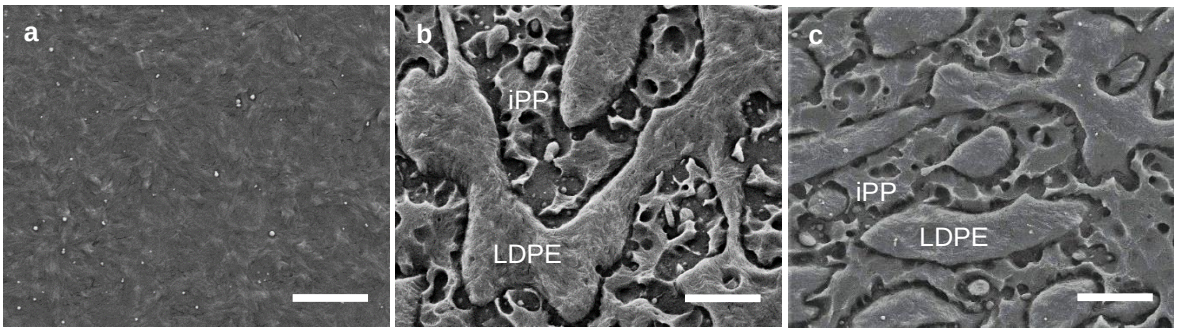

Figure 33. SEM micrographs of the cryofractured, etched and sputtered surfaces of **(a)** the LDPE nanocomposite, **(b)** the $SEBS_B$:iPP:LDPE ternary blend, and **(c)** the $SEBS_B$:iPP:LDPE:Al_2O_3 ternary blend nanocomposite (scale bar = 2 μm).

Chapter 10

Conclusion and Outlook

Thermoplastic blends based on LDPE and iPP prepared by reactive compounding and blending have been explored in the thesis. Both routes have led to material concepts that facilitate the design of insulation materials for high voltage cables.

Reactive compounding with iPP-*graft*-MA and p(E-*stat*-GMA) was shown to be a viable route for compatibilising iPP:LDPE blends. The p(E-*stat*-GMA):iPP-*graft*-MA:LDPE ternary blend investigated was a thermoplastic material that possessed thermomechanical properties superior to neat LDPE despite a relatively low iPP content. This material also displayed a low DC electrical conductivity σ_{DC} comparable to reference XLPE despite the presence of polar groups. It would therefore be worth further exploring the reactive compounding route for the development of HVDC cable insulation materials, for instance using alternative reaction schemes that are less moisture sensitive. Further, reversible crosslinking of polymer blends could also be of interest. Crosslinked polymer blends that undergo de-crosslinking at compounding temperatures (below degradation temperatures) but remain crosslinked at cable operation temperatures allow for good thermomechanical properties and also reprocessability by melting. Such materials should also be less prone to phase separation if the polymers in the blend are highly miscible. Since a low σ_{DC} was maintained in the p(E-*stat*-GMA):iPP-*graft*-MA:LDPE ternary blend described in the thesis, it may be possible to obtain a low σ_{DC} for reversibly crosslinked materials.

The compounding of iPP and LDPE with SEBS led to thermoplastic ternary blends where blend compositions could be tailored to achieve an appropriate stiffness (both below and at cable operation temperatures), robustness against small changes in processing conditions, and a low DC electrical conductivity, without inordinately compromising on thermal conductivity. It was further demonstrated that additive amounts of surface-modified Al_2O_3 nanoparticles could further reduce σ_{DC} of these ternary blends without compromising on mechanical properties. This introduces another variable that can be tuned to achieve improved material performance on all fronts for such formulations. To further increase the potential of these blends (with and without Al_2O_3 nanoparticles), it would be valuable to better understand the mechanism behind the increase in *E'* and creep resistance above T_m^{LDPE} observed in blends with SEBS. It would also be useful to have a systematic study on how/whether the styrene content, molecular weight, comonomers, molecular architecture and molecular weights of styrenic block copolymers affect the different properties of these ternary blends. A deeper understanding on how these copolymers affect blend properties will facilitate the attainment of materials that are well-suited for high voltage cable insulation applications.

Since much larger scales are used in cable production, it is important to investigate if the properties of the blends vary when upscaled. Therefore, a $SEBS_B$:iPP:LDPE ternary blend was compounded at a scale of 2 kg and characterised. The upscaled $SEBS_B$:iPP:LDPE ternary blend demonstrated an *E'* that was similar to reference random heterophasic PP (hPP) at 40 °C, and exhibited not only *E'* greater than hPP above T_m^{LDPE} but also a rubber plateau that exists to even higher temperatures than hPP (matching iPP) (Figure 34). In other words, this blend matches hPP in terms of softness at low temperatures, and compared to hPP is expected to be more resistant to mechanical stresses at elevated temperatures and over a wider range of temperatures. Furthermore, the ternary blend displays $\sigma_{DC} \sim 2 \cdot 10^{-15}$ S m^{-1} at 70 °C and 30 kV mm^{-1}. This is approximately an order of magnitude lower than that of neat LDPE $\sigma_{DC} \sim 2 \cdot 10^{-14}$

S m^{-1}, and lower than σ_{DC} of both references XLPE and hPP (Figure 35a). In fact, σ_{DC} of the ternary blend nearly matches the highly insulating iPP, which features a $\sigma_{DC} \sim 1 \cdot 10^{-15}$ S m^{-1} at 70 °C and 30 kV mm^{-1}. Furthermore, the ternary blend demonstrates a thermal conductivity κ ~ 0.30 W $m^{-1}K^{-1}$, which is significantly higher than κ ~ 0.24 W $m^{-1}K^{-1}$ measured for hPP, and approaches κ ~ 0.33 W $m^{-1}K^{-1}$ for XLPE (Figure 35b). These results mean that this ternary blend may potentially aid the design of cables that can sustain higher voltages and hence transmit more electrical power than current HVDC cables. In addition, the DMA curves of the blend compounded at 180 °C and 200 °C showed very similar properties when studied with DMA, DC electrical conductivity and thermal conductivity measurements, demonstrating the robustness of this ternary blend towards small changes in processing conditions.

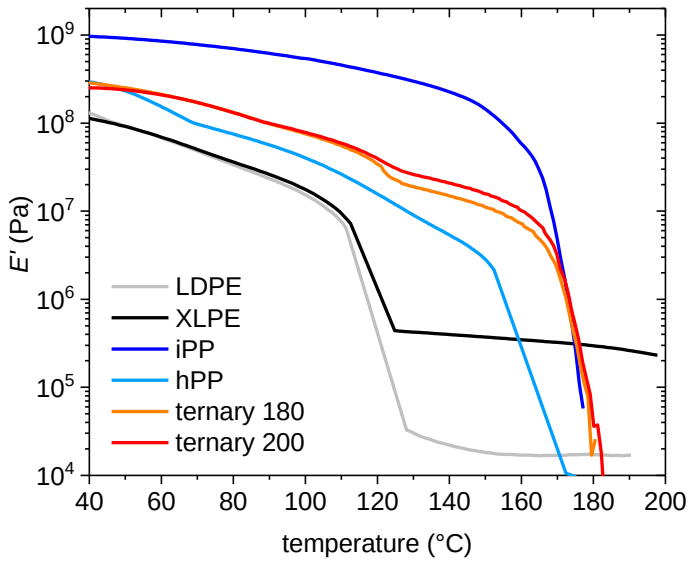

Figure 34. Storage modulus *E'* measured with DMA as a function of temperature, of LDPE (grey), XLPE (black), iPP (blue), and hPP (sky blue), and the upscaled 20:38:42 $SEBS_B$:iPP:LDPE ternary blend compounded at 180 °C (orange) and 200 °C (red).

Compounding of ternary blends was done by Johan Landberg (Research Institutes of Sweden (RISE)) using a Coperion ZSK 26 K 10.6 twin screw extruder at RISE.

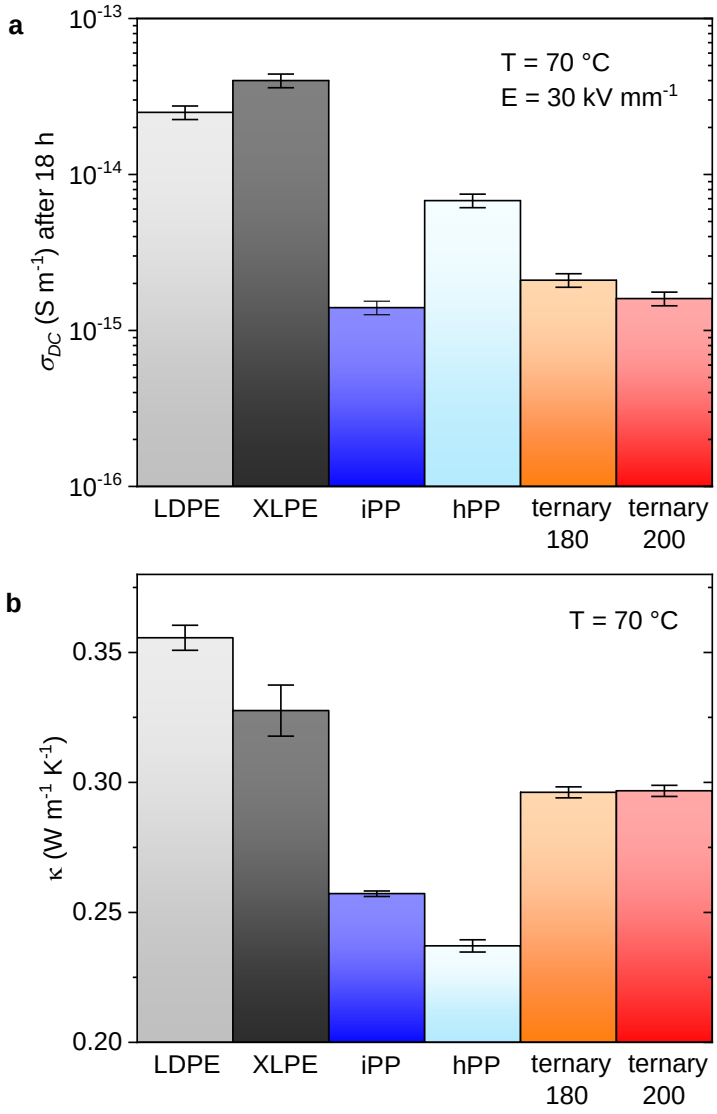

Figure 35. (a) σ_{DC} obtained after 18 h at 70 °C and an electric field of 30 kV mm^{-1} (error bars are based on ~10% error estimated based on three measurements on neat LDPE (data from *paper I*)), and **(b)** κ at 70 °C (error bars are based on the standard deviation calculated from 5 measurements of each sample), of LDPE (grey), XLPE (black), iPP (blue), hPP (sky blue), and the upscaled 20:38:42 SEBS$_B$:iPP:LDPE ternary blend compounded at 180 °C (orange) and 200 °C (red). *DC conductivity measurements were done by Azadeh Soroudi (Chalmers).*

To further test the suitability of the investigated ternary blends for HVDC cable insulation, thermopressure tests designed to simulate the conditions experienced by a cable insulation material can be conducted to assess the mechanical performance of the material at elevated temperatures. DC conductivity measurements at even higher temperatures and further electrical characterisation such as breakdown strength should also be carried out. Additionally, ageing studies would be valuable for evaluating how prone such materials are to gradual phase separation and degradation that can cause deterioration in material properties (eg. mechanical, electrical) over time under cable operation conditions. The long-term stability of these materials would ultimately also influence their recyclability (by reprocessing in the melt) at the end of life of cables.

The material concepts described in this thesis show potential for the development of novel insulation materials for HVDC cables. From a practical point of view, the introduction of thermoplastics for HVDC cable insulation may initially be challenging due to the lack of a track record (so far, the success of thermoplastics has only been seen in medium voltage alternating current cables, whereas XLPE is a well-established insulation material for HVDC cables). Further, production assets have already been extensively developed and optimised for XLPE, but the manufacturing of thermoplastic-insulated HVDC cables will require new and/or adapted production assets – the time and resources needed for this will not be trivial. However, with further investigations, testing and optimisation, the material concepts explored here could contribute to a more sustainable future.

Acknowledgements

This thesis would not exist if it were based on my solo efforts in an isolated world. In fact, I would have been completely lost at the start of my project if I had been left to my own devices. Having done my undergraduate studies in chemistry, I was only used to glassware, so working with 'metal machinery' like the compounder and the hot press was a whole new world to me (in addition to being in a new country). I am indebted to my supervisors, colleagues, collaborators, teachers, friends and my experiences throughout my PhD journey in Sweden, for the progress I have made since I started my PhD, both from a scientific point of view and also in terms of personal development (both have been crucial for bringing my thesis to fruition).

First and foremost, I would like to express my immense gratitude to my main supervisor Christian Müller. Thank you for taking the leap of faith to hire me as a PhD student on this project despite my lack of knowledge and experience in polymer processing and characterisation prior to starting my PhD, and for always being so helpful and supportive, especially in the beginning when I was climbing the steep learning curve. I have learnt so much from you about polymers, presentation of data and writing, and am also grateful for other non-scientific help, in particular how you helped me realise that I can and should believe in myself more (even though you often send back manuscript drafts covered in red).

My co-supervisor Per-Ola Hagstrand has also been extremely supportive throughout my PhD. Per-Ola, thank you so much for always being so welcoming to my questions, taking time to discuss my data and ideas and offering your insights (especially from the industrial point of view). I have really enjoyed our discussions – I greatly appreciate your open-minded and non-judgemental attitude, which has allowed me to express my ideas and thoughts freely even if some of them seemed somewhat silly, and I think this made our discussions even more interesting and enlightening.

I would also like to thank other Borealis colleagues Thomas Gkourmpis and Martin Anker. Your input and support have been invaluable to the development of our project, and I hope that our project can be taken further in future. Borealis AB has provided expertise, guidance, financial support and key materials for my project, which I am very grateful for.

Several colleagues have also made important scientific contributions to my thesis. Massi, thank you for guiding me in my first study. Amir, thank you for helping with electrical measurements, your tips for SEM microscopy, and our scientific discussions. Xiangdong, thank you for helping with the DC-conductivity setup, without which we would not have been able to obtain electrical characterisation of our materials. Azadeh, thank you for helping with electrical measurements, the experiments regarding upscaling (and thank you Johan for compounding my ternary blends in the large compounder at RISE) and the nanocomposites, and for our interesting discussions. Thank you also to Anja for helping with the DC-conductivity setup, X-ray measurements, the TMA, and for all your help when running into issues with instruments. Ida, thank you as well for help with X-ray measurements (and 3D printing although the Pikachu did not end up in the final version of *paper I*). Furthermore, I would like to thank Andrey for guiding me with the use of the HotDisk for thermal conductivity measurements, Anders and Stefan for guiding me when I first used the SEM, Anna P for all your guidance with the DMA, the rheometer and sample etching, and Emmy for showing me how to use the Linkam stage for the FT-IR spectrometer. A big thank you to Jakob and Marcus as well for all your hard work and our interesting discussions on the SEBS project (and for being such a pleasure to work with – I learnt a lot from working with you)!

Additionally, I would like to thank the Chalmers Materials Analysis Laboratory (CMAL) for their infrastructures used for materials characterisation, the Research Institutes of Sweden (RISE) for allowing us to use your compounder for the upscaling project, and to KRATON for sending a variety of styrenic copolymers for our studies.

Apart from scientific collaborations, I am also grateful to friends and colleagues at Chalmers who have supported and inspired me throughout my PhD journey:

Thank you Massi, Jason and Renee for helping me settle in during my first years at Chalmers by being so friendly, fun and welcoming. Although all of you left Chalmers before me, you have continued offering me support, encouragement and advice. I really appreciate it.

Anna (Peterson), it is such a shame that we never got to collaborate in scientific projects (officially). I have really enjoyed our discussions (scientific and non-scientific), and you have been such an inspiration to me. Your support, encouragement and contagious positive energy have helped me in my work and life. I will also never forget how you looked out for me (especially on our work trips abroad), like when you saved me from the dog and snake in Italy!

Anja, thank you so much for your wisdom, encouragement, support, advice, and for being a great listener. You have helped me a lot through the bumpier periods of my PhD journey. Thank you too for helping with the translation of my popular science text at the back of this thesis.

Emmy, thank you too for helping with the translation of my popular science text, and also for being a great and fun colleague *and* friend who makes coming to work even more fun! Thank you Sepideh too for the same reason, but I would also like to formally thank you for taking and editing my photograph for the back cover of my thesis.

Last but not least, thank you Sozan my ‘bro’ for being such a great office mate! It has been so much fun sharing an office with you, and I am proud of us for still managing to get work done.

Once again, thank you to everyone mentioned here for their support, and thank you also to the whole Müller group (past and present) and everyone else on floor 8 Applied Chemistry for the wonderful working environment that has undoubtedly made my PhD journey smoother and more enjoyable.

References

1. *Report of the World Commission on Environment and Development: Our Common Future*. Oxford University Press: Oxford, 1987.

2. Purvis, B.; Mao, Y.; Robinson, D., Three pillars of sustainability: in search of conceptual origins. *Sustain. Sci.* **2019,** *14*, 681-695.

3. THE 17 GOALS | Sustainable Development. https://sdgs.un.org/goals (accessed 16 June 2021).

4. Mazzanti, G.; Marzinotto, M., *Extruded Cables for High-Voltage Direct-Current Transmission*. Wiley: New Jersey, 2013.

5. Worzyk, T., Applications of Submarine Power Cables. In *Submarine Power Cables: Design, Installation, Repair, Environmental Aspects*, Springer Berlin Heidelberg: Berlin, Heidelberg, 2009; pp 1-8.

6. Okba, M. H.; Saied, M. H.; Mostafa, M. Z.; Abdel-Moneim, T. M. *High voltage direct current transmission - A review, part I*, 2012 IEEE Energytech, IEEE: Cleveland, OH, USA, 2012; pp 1-7.

7. *HVDC extruded cable*; Svenska kraftnät: 2018.

8. Chen, G.; Hao, M.; Xu, Z.; Vaughan, A.; Cao, J.; Wang, H., Review of high voltage direct current cables. *CSEE J. Power Energy Syst.* **2015,** *1*, 9-21.

9. Fothergill, J. C. *The coming of Age of HVDC extruded power cables*, 2014 IEEE Electr. Insul. Conf. (EIC), Philadelphia, PA, USA, 2014; pp 124-137.

10. Ardelean, M.; Minnebo, P., HVDC Submarine Power Cables in the World: State-of-the-Art Knowledge. EUR 27527. Publications Office of the European Union: Netherlands, 2015.

11. Tvaronavičienė, M.; Baublys, J.; Raudeliūnienė, J.; Jatautaitė, D., Global energy consumption peculiarities and energy sources: Role of renewables. In *Energy Transformation*

Towards Sustainability, Tvaronavičienė, M.; Ślusarczyk, B., Eds. Elsevier: Amsterdam, Netherlands, 2020; pp 1-49.

12. Rafiee, A.; Khalilpour, K. R., Renewable Hybridization of Oil and Gas Supply Chains. In *Polygeneration with Polystorage for Chemical and Energy Hubs*, 1st ed.; Khalilpour, K. R., Ed. Elsevier: London UK, 2019; pp 331-372.

13. Gielen, D.; Boshell, F.; Saygin, D.; Bazilian, M. D.; Wagner, N.; Gorini, R., The role of renewable energy in the global energy transformation. *Energy Strategy Rev.* **2019,** *24*, 38-50.

14. Abulfotuh, F., Energy efficiency and renewable technologies: the way to sustainable energy future. *Desalination* **2007,** *209*, 275-282.

15. del Río, P., Analysing the interactions between renewable energy promotion and energy efficiency support schemes: The impact of different instruments and design elements. *Energy Policy* **2010,** *38*, 4978-4989.

16. Owusu, P. A.; Asumadu-Sarkodie, S., A review of renewable energy sources, sustainability issues and climate change mitigation. *Cogent Eng.* **2016,** *3*, 1167990.

17. Abbasi, T.; Premalatha, M.; Abbasi, S. A., The return to renewables: Will it help in global warming control? *Renew. Sustain. Energy Rev.* **2011,** *15*, 891-894.

18. Moriarty, P.; Honnery, D., What is the global potential for renewable energy? *Renew. Sustain. Energy Rev.* **2012,** *16*, 244-252.

19. *Climate Change 2014: Synthesis Report. Contribution of Working Groups I, II and III to the Fifth Assessment Report of the Intergovernmental Panel on Climate Change*; Geneva, Switzerland, 2014; p 151.

20. Quaschning, V., *Understanding Renewable Energy Systems*. 2nd ed.; Routledge: London, 2016.

21. Denholm, P.; Ela, E.; Kirby, B.; Milligan, M. *Role of Energy Storage with Renewable Electricity Generation*; United States, 2010.

22. Jewell, W. T. *Electric Industry Infrastructure for Sustainability: Climate Change and Energy Storage*, 2007 IEEE Power Energy Soc. Gen. Meet., IEEE: Tampa, FL, USA, 2007; pp 1-3.

23. Alamri, B. R.; Alamri, A. R. *Technical review of energy storage technologies when integrated with intermittent renewable energy*, 2009 Int. Conf. on Sustainable Power Generation and Supply, IEEE: Nanjing, China, 2009; pp 1-5.

24. Montanari, G. C.; Morshuis, P. H. F.; Zhou, M.; Stevens, G. C.; Vaughan, A. S.; Han, Z.; Li, D., Criteria influencing the selection and design of HV and UHV DC cables in new network applications. *High Volt.* **2018,** *3*, 90-95.

25. Jeroense, M. *HVDC, the next generation of transmission highlights with focus on extruded cable systems*, Proc. Int. Symp. Electr. Insul. Mater., IEEE: Yokkaichi, Japan, 2008; pp 10-15.

26. Ghorbani, H.; Jeroense, M.; Olsson, C.; Saltzer, M., HVDC Cable Systems—Highlighting Extruded Technology. *IEEE Trans. Power Deliv.* **2014,** *29*, 414-421.

27. Majumder, R.; Bartzsch, C.; Kohnstam, P.; Fullerton, E.; Finn, A.; Galli, W., Magic Bus: High-Voltage DC on the New Power Transmission Highway. *IEEE Power Energy Mag.* **2012,** *10*, 39-49.

28. Lundberg, P.; Callavik, M.; Bahrman, M.; Sandeberg, P., Platforms for Change: High-Voltage DC Converters and Cable Technologies for Offshore Renewable Integration and DC Grid Expansions. *IEEE Power Energy Mag.* **2012,** *10*, 30-38.

29. Colla, L.; Zaccone, E. *HVDC Land and Submarine Cables in the Mediterranean Area*, 2018 AEIT Int. Annu. Conf., IEEE: Bari, Italy, 2018; pp 1-6.

30. Zhou, Y.; Peng, S.; Hu, J.; He, J., Polymeric insulation materials for HVDC cables: Development, challenges and future perspective. *IEEE Trans. Dielectr. Electr. Insul.* **2017,** *24*, 1308-1318.

31. Rüter, F.; Parpal, J. L.; Swingler, S. G., A review of HVDC extruded cable systems. In *Int. Council on Large Electric Systems (CIGRÉ)*, Paris. France: 2000; pp Paper P2-03.

32. Wei, Y.; Han, W.; Li, G.; Lei, Q.; Fu, M.; Hao, C.; Zhang, G., Research progress of semiconductive shielding layer of HVDC cable. *High Volt.* **2020,** *5*, 1-6.

33. Vahedy, V., Polymer insulated high voltage cables. *IEEE Electr. Insul. Mag.* **2006,** *22*, 13-18.

34. Beddard, A.; Barnes, M. *HVDC cable modelling for VSC-HVDC applications*, 2014 IEEE PES General Meeting | Conference & Exposition, National Harbor, MD, USA, 2014; pp 1-5.

35. Hanley, T. L.; Burford, R. P.; Fleming, R. J.; Barber, K. W., A general review of polymeric insulation for use in HVDC cables. *IEEE Electr. Insul. Mag.* **2003,** *19*, 13-24.

36. Fazal, A.; Hao, M.; Vaughan, A. S.; Chen, G.; Cao, J.; Wang, H. *The effect of composition and processing on electric characteristics of XLPE in HVDC cable applications*, 2016 IEEE Electr. Insul. Conf. (EIC), IEEE: Montreal, QC, Canada, 2016; pp 440-443.

37. Farkas, A.; Olsson, C.-O.; Dominguez, G.; Englund, V.; Hagstrand, P.-O.; Nilsson, U. H. *Development of High Performance Polymeric Materials for HVDC Cables*, Jicable'11 - 8th Int. Conf. on Insulated Power Cables Versailles, France, 2011.

38. Andersson, M. G.; Hynynen, J.; Andersson, M. R.; Englund, V.; Hagstrand, P.-O.; Gkourmpis, T.; Müller, C., Highly Insulating Polyethylene Blends for High-Voltage Direct-Current Power Cables. *ACS Macro Lett.* **2017,** *6*, 78-82.

39. Jordan, J. L.; Casem, D. T.; Bradley, J. M.; Dwivedi, A. K.; Brown, E. N.; Jordan, C. W., Mechanical Properties of Low Density Polyethylene. *J. Dyn. Behav. Mater.* **2016,** *2*, 411-420.

40. Andrews, T.; Hampton, R. N.; Smedberg, A.; Wald, D.; Waschk, V.; Weissenberg, W., The role of degassing in XLPE power cable manufacture. *IEEE Electr. Insul. Mag.* **2006,** *22*, 5-16.

41. Hosier, I. L.; Vaughan, A. S.; Pye, A.; Stevens, G. C., High performance polymer blend systems for HVDC applications. *IEEE Trans. Dielectr. Electr. Insul.* **2019,** *26*, 1197-1203.

42. Du, B. X.; Han, C.; Li, J.; Li, Z., Effect of voltage stabilizers on the space charge behavior of XLPE for HVDC cable application. *IEEE Trans. Dielectr. Electr. Insul.* **2019,** *26*, 34-42.

43. Orton, H., History of underground power cables. *IEEE Electr. Insul. Mag.* **2013,** *29*, 52-57.

44. Liu, Y.; Cao, X.; Chen, G., Electrical tree initiation in XLPE cable insulation under constant DC, grounded DC, and at elevated temperature. *IEEE Trans. Dielectr. Electr. Insul.* **2018,** *25*, 2287-2295.

45. Nilsson, U. H.; Andersson, J.; Englund, V.; Eriksson, V.; Hagstrand, P.-O.; Smedberg, A. *The role and measurement of DC conductivity for HVDC cable insulation materials*, Conf. Electr. Insul. Dielectr. Phenom. CEIDP, IEEE: Ann Arbor, MI, USA, 2015; pp 31-34.

46. Peschke, E.; Olshausen, R. V., *Cable Systems for High and Extra-High Voltage: Development, Manufacture, Testing, Installation and Operation of Cables and Their Accessories*. Wiley-VCH Verlag GmbH: Munich, 2000.

47. Kuffel, E.; Zaengl, W. S.; Kuffel, J., *High Voltage Engineering: Fundamentals*. 2 ed.; Butterworth-Heinemann: Jordan Hill, Oxford, 2000.

48. Lagrotteria, G.; Pietribiasi, D.; Marelli, M. *HVDC Cables - The technology boost*, 2019 AEIT HVDC Int. Conf., IEEE: Florence, Italy, 2019; pp 1-5.

49. Xiao, M.; Du, B. X., Review of high thermal conductivity polymer dielectrics for electrical insulation. *High Volt.* **2016,** *1*, 34-42.

50. Du, B. X.; Kong, X. X.; Cui, B.; Li, J., Improved ampacity of buried HVDC cable with high thermal conductivity LDPE/BN insulation. *IEEE Trans. Dielectr. Electr. Insul.* **2017,** *24*, 2667-2676.

51. Huang, X.; Zhang, J.; Jiang, P.; Tanaka, T., Material progress toward recyclable insulation of power cables part 2: Polypropylene-based thermoplastic materials. *IEEE Electr. Insul. Mag.* **2020,** *36*, 8-18.

52. Wald, D.; Igbinovia, F. O.; Raikisto, P. *Thermoplastic Insulation System for Power Cables*, 2020 IEEE PES/IAS PowerAfrica, IEEE: Nairobi, Kenya, 2020; pp 1-5.

53. Prysmian secures approx. €500M SuedOstLink cable corridor project in Germany. Prysmian Group: Milan, Italy, 2020.

54. Amprion selects ±525 kV HVDC extruded cable system, providing reliability and sustainability. Prysmian Group: Milan, Italy, 2020.

55. Andritsch, T.; Vaughan, A.; Stevens, G. C., Novel insulation materials for high voltage cable systems. *IEEE Electr. Insul. Mag.* **2017,** *33*, 27-33.

56. Gustafsson, B.; Boström, J.-O.; Dammert, R. C., Stabilization of peroxide crosslinked polyethylene. *Angew. Makromol. Chem.* **1998,** *261-262*, 93-99.

57. Nylander, P.; Lindbom, L., Methods to predict processing behaviour for cross linking polyolefin compounds by extrusion and Rheometer. *Annu. Trans. Nord. Rheol. Soc.* **2004,** *12*.

58. Grigore, M. E., Methods of Recycling, Properties and Applications of Recycled Thermoplastic Polymers. *Recycling* **2017,** *2*, 24.

59. Huuva, R.; Ribarits, E. *Recycling XLPE from cable waste*, Jicable'19 - 10th Int. Conf. on Insulated Power Cables, Versailles, France, 2019.

60. Boss, A.; Boström, J.-O.; Nilsson, P.-H.; Farkas, A.; Eriksson, A.; Rasmussen, E.; Svenningsson, E.; Dalesjö, M.; Johansson, A. *New Technology for Recycling of Plastics from Cable Waste* Jicable'11 - 8th Int. Conf. on Insulated Power Cables, Versailles, France, 2011.

61. Sekiguchi, Y.; Ohkawa, N.; Nojo, H.; Hashimoto, S. *Development of Recycling Technology of XLPE*, Jicable'07 - 7th Int. Conf. on Power Insulated Cables, Versailles, France, 2007.

62. Boss, A.; Landberg, J. *Recycling and Circularity in Power Distribution Cables: A fact-based study comparing market sourced MV XLPE and PP-TPE insulated cables*; Research Institutes of Sweden (RISE): 2021.

63. Lindqvist, K.; Andersson, M.; Boss, A.; Oxfall, H., Thermal and Mechanical Properties of Blends Containing PP and Recycled XLPE Cable Waste. *J. Polym. Environ.* **2019,** *27*, 386-394.

64. Tokuda, S.; Horikawa, S.; Negishi, K.; Uesugi, K.; Hirukawa, H., Thermoplasticizing Technology for the Recycling of Crosslinked Polyethylene. *Furukawa Rev.* **2003,** *23*.

65. Lu, C.; Zhang, X.; Zhang, W., Recycling and processing of several typical crosslinked polymer scraps with enhanced mechanical properties based on solid-state mechanochemical milling. *AIP Conf. Proc.* **2015,** *1664*, 150008.

66. Hosier, I. L.; Vaughan, A. S.; Swingler, S. G., An investigation of the potential of polypropylene and its blends for use in recyclable high voltage cable insulation systems. *J. Mater. Sci.* **2011,** *46*, 4058-4070.

67. Hosier, I. L.; Cozzarini, L.; Vaughan, A. S.; Swingler, S. G., Propylene based systems for high voltage cable insulation applications. *J. Phys.: Conf. Ser.* **2009,** *183*, 012015.

68. Belli, S.; Perego, G.; Caimi, L.; Bareggi, A.; Crisci, V.; Pozzati, G.; Franchi, S.; Albertini, M.; Donazzi, F.; Zaccone, E.; Valls, A. *P-Laser: 10.000 km of installed cables based on a worldwide new technology*, Jicable'11 - 8th Int. Conf. on Insulated Power Cables, Prysmian Group: Versailles, France, 2011.

69. Montanari, G. C.; Seri, P.; Lei, X.; Ye, H.; Zhuang, Q.; Morshuis, P.; Stevens, G.; Vaughan, A., Next generation polymeric high voltage direct current cables—A quantum leap needed? *IEEE Electr. Insul. Mag.* **2018,** *34*, 24-31.

70. Andersson, M. G.; Hynynen, J.; Andersson, M. R.; Hagstrand, P.-O.; Gkourmpis, T.; Müller, C., Additive-like amounts of HDPE prevent creep of molten LDPE: Phase-behavior and thermo-mechanical properties of a melt-miscible blend. *J. Polym. Sci. B: Polym. Phys* **2017,** *55*, 146-156.

71. Andersson, M. G.; Städler, R.; Hagstrand, P.-O.; Gkourmpis, T.; Andersson, M. R.; Müller, C., Influence of Molecular Weight on the Creep Resistance of Almost Molten Polyethylene Blends. *Macromol. Chem. Phys.* **2018,** *219*, 1700072.

72. Green, C. D.; Vaughan, A. S.; Stevens, G. C.; Sutton, S. J.; Geussens, T.; Fairhurst, M. J., Recyclable power cable comprising a blend of slow-crystallized polyethylenes. *IEEE Trans. Dielectr. Electr. Insul.* **2013,** *20*, 1-9.

73. Hosier, I. L.; Vaughan, A. S.; Swingler, S. G., Structure–property relationships in polyethylene blends: the effect of morphology on electrical breakdown strength. *J. Mater. Sci.* **1997,** *32*, 4523-4531.

74. Hosier, I. L.; Vaughan, A. S.; Swingler, S. G., On the effects of morphology and molecular composition on the electrical strength of polyethylene blends. *J. Polym. Sci. B: Polym. Phys.* **2000,** *38*, 2309-2322.

75. Dodd, S. J.; Champion, J. V.; Zhao, Y.; Vaughan, A. S.; Sutton, S. J.; Swingler, S. G., Influence of morphology on electrical treeing in polyethylene blends. *IEE Proc. Sci. Meas. Tech.* **2003,** *150*, 58-64.

76. Nilsson, F.; Karlsson, M.; Gedde, U. W.; Kádár, R.; Gaska, K.; Müller, C.; Hagstrand, P.-O.; Olsson, R. T.; Hedenqvist, M. S.; Gkourmpis, T., Nanocomposites and polyethylene blends: two potentially synergistic strategies for HVDC insulation materials with ultra-low electrical conductivity. *Compos. B. Eng* **2021,** *204*, 108498.

77. Fan, Z. J.; Williams, M. C.; Choi, P., A molecular dynamics study of the effects of branching characteristics of LDPE on its miscibility with HDPE. *Polymer* **2002,** *43*, 1497-1502.

78. Sarkhel, G.; Banerjee, A.; Bhattacharya, P., Rheological and Mechanical Properties of LDPE/HDPE Blends. *Polym. Plast. Technol. Eng.* **2006,** *45*, 713-718.

79. Freed, K. F.; Dudowicz, J., Influence of Short Chain Branching on the Miscibility of Binary Polymer Blends: Application to Polyolefin Mixtures. *Macromolecules* **1996,** *29*, 625-636.

80. Hill, M. J.; Barham, P. J.; Keller, A.; Rosney, C. C. A., Phase segregation in melts of blends of linear and branched polyethylene. *Polymer* **1991,** *32*, 1384-1393.

81. Martínez-Salazar, J.; Cuesta, M. S.; Plans, J., On phase separation in high- and low-density polyethylene blends: 1. Melting-point depression analysis. *Polymer* **1991,** *32*, 2984-2988.

82. Malpass, D. B., *Introduction to Industrial Polyethylene: Properties, Catalysts, and Processes*. Wiley-Scrivener Publishing LLC: Salem, Massachusetts, 2010.

83. Yu, S.; Lee, S. H.; Han, J. A.; Ahn, M. S.; Park, H.; Han, S. W.; Lee, D. H., Insulative ethylene-propylene copolymer-nanostructured polypropylene for high-voltage cable insulation applications. *Polymer* **2020,** *202*, 122674.

84. Diao, J.; Huang, X.; Jia, Q.; Liu, F.; Jiang, P., Thermoplastic isotactic polypropylene/ethylene-octene polyolefin copolymer nanocomposite for recyclable HVDC cable insulation. *IEEE Trans. Dielectr. Electr. Insul.* **2017,** *24*, 1416-1429.

85. Green, C. D.; Vaughan, A. S., Thermoplastic Cable Insulation Comprising a Blend of Isotactic Polypropylene and a Propylene-ethylene Copolymer. *IEEE Trans. Dielectr. Electr. Insul.* **2015,** *22*, 639-648.

86. Hong, S. K.; Lee, S. H.; Han, J. A.; Ahn, M. S.; Park, H.; Han, S. W.; Lee, D. H.; Yu, S., Polypropylene-based soft ternary blends for power cable insulation at low-to-high temperature. *J. Appl. Polym. Sci.* **2021**, 51619.

87. Huang, X.; Fan, Y.; Zhang, J.; Jiang, P., Polypropylene based thermoplastic polymers for potential recyclable HVDC cable insulation applications. *IEEE Trans. Dielectr. Electr. Insul.* **2017,** *24*, 1446-1456.

88. Kim, D. W.; Yoshino, K.; Inoue, T.; Abe, M.; Uchikawa, N., Influence of Morphology on Electrical Properties of Syndiotactic Polypropylene Compared with Those of Isotactic Polypropylene. *Jpn. J. Appl. Phys.* **1999,** *38*, 3580–3584.

89. Zhou, Y.; He, J.; Hu, J., Evaluation of Polypropylene/Polyolefin Elastomer Blends for Potential Recyclable HVDC Cable Insulation Applications. *IEEE Trans. Dielectr. Electr. Insul.* **2015,** *22*, 673-681.

90. Belli, S.; Perego, G.; Bareggi, A.; Caimi, L.; Donazzi, F.; Zaccone, E., P-Laser Breakthrough in power cable systems. In *IEEE Int. Sym. Elec. In.*, IEEE: San Diego, CA, 2010; pp 1-5.

91. Ouyang, Y.; Pourrahimi, A. M.; Lund, A.; Xu, X.; Gkourmpis, T.; Hagstrand, P.-O.; Müller, C., High-temperature creep resistant ternary blends based on polyethylene and polypropylene for thermoplastic power cable insulation. *J. Polym. Sci.* **2021,** *59*, 1084-1094

92. Cowie, J. M. G., Glass transition temperatures of stereoblock, isotactic and atactic polypropylenes of various chain lengths. *Eur. Polym. J.* **1973,** *9*, 1041-1049.

93. Hosier, I. L.; I, S. R.; Vaughan, A. S.; Swingler, S. G., Morphology, thermal, mechanical and electrical properties of propylene-based materials for cable applications. In *Conf. Rec. IEEE Int. Symp. Electr. Insul.*, IEEE: Vancouver, BC, Canada, 2008; pp 502-505.

94. Zhang, C.; Mizutani, T.; Kaneko, K.; Mori, T.; Ishioka, M., Space charge behaviors of low-density polyethylene blended with polypropylene copolymer. *Polymer* **2002,** *43*, 2261-2266.

95. Zhang, C.; Mori, T.; Mizutani, T.; Ishioka, M.; Cheng, Y., Morphology and electrical breakdown properties of LDPE-polypropylene copolymer blends. *J. Polym. Sci., Part B: Polym. Phys.* **2001,** *39*, 1741-1748.

96. Ouyang, Y.; Mauri, M.; Pourrahimi, A. M.; Östergren, I.; Lund, A.; Gkourmpis, T.; Prieto, O.; Xu, X.; Hagstrand, P.-O.; Müller, C., Recyclable Polyethylene Insulation via Reactive Compounding with a Maleic Anhydride-Grafted Polypropylene. *ACS Appl. Polym. Mater.* **2020,** *2*, 2389–2396.

97. Dabbak, S. Z. A.; Illias, H. A.; Ang, B. C.; Latiff, N. A. A.; Makmud, M. Z. H., Electrical Properties of Polyethylene/Polypropylene Compounds for High-Voltage Insulation. *Energies* **2018,** *11*, 1448.

98. Nolley, E.; Barlow, J. W.; Paul, D. R., Mechanical properties of polypropylene-low density polyethylene blends. *Polym. Eng. Sci.* **1980,** *20*, 364-369.

99. Teh, J. W., Structure and properties of polyethylene–polypropylene blend. *J. Appl. Polym. Sci.* **1983,** *28*, 605-618.

100. Miles, I. S.; Zurek, A., Preparation, structure, and properties of two-phase co-continuous polymer blends. *Polym. Eng. Sci.* **1988,** *28*, 796-805.

101. Menard, K. P., *Dynamic Mechanical Analysis - A Practical Introduction*. CRC Press LLC: 1999.

102. Chartoff, R. P.; Menczel, J. D.; Dillman, S. H., Dynamic Mechanical Analysis (DMA). In *Thermal Analysis of Polymers*, 2009; pp 387-495.

103. Khonakdar, H. A.; Morshedian, J.; Wagenknecht, U.; Jafari, S. H., An investigation of chemical crosslinking effect on properties of high-density polyethylene. *Polymer* **2003,** *44*, 4301-4309.

104. Smedberg, A.; Hjertberg, T.; Gustafsson, B., The role of entanglements in network formation in unsaturated low density polyethylene. *Polymer* **2004,** *45*, 4867-4875.

105. Mauri, M.; Hofmann, A. I.; Gómez-Heincke, D.; Kumara, S.; Masoud Pourrahimi, A.; Ouyang, Y.; Hagstrand, P.-O.; Gkourmpis, T.; Xu, X.; Prieto, O.; Müller, C., Click chemistry-type crosslinking of a low-conductivity polyethylene copolymer ternary blend for power cable insulation. *Polym. Int.* **2020,** *69*, 404-412.

106. Torres, N.; Robin, J. J.; Boutevin, B., Study of Compatibilization of HDPE–PET Blends by Adding Grafted or Statistical Copolymers. *J. Appl. Polym. Sci.* **2001,** *81*, 2377-2586.

107. Wei, Q.; Chionna, D.; Galoppini, E.; Pracella, M., Functionalization of LDPE by Melt Grafting with Glycidyl Methacrylate and Reactive Blending with Polyamide-6. *Macromol. Chem. Phys.* **2003,** *204*, 1123–1133.

108. Chiono, V.; Filippi, S.; Yordanov, H.; Minkova, L.; Magagnini, P., Reactive compatibilizer precursors for LDPE/PA6 blends. III: ethylene–glycidylmethacrylate copolymer. *Polymer* **2003,** *44*, 2423-2432.

109. Garcia, R. D. B.; Keromnes, L.; Goutille, Y.; Cassagnau, P.; Fenouillot, F.; Chaumont, P., Structural evolution of a constrained epoxy functional polyethylene network crosslinked by a bio-based reactant. *Eur. Polym. J.* **2014,** *61*, 186-196.

110. Mauri, M.; Peterson, A.; Senol, A.; Elamin, K.; Gitsas, A.; Hjertberg, T.; Matic, A.; Gkourmpis, T.; Prieto, O.; Müller, C., Byproduct-free curing of a highly insulating polyethylene copolymer blend: an alternative to peroxide crosslinking. *J. Mater. Chem. C* **2018,** *6*, 11292-11302.

111. Mauri, M.; Svenningsson, L.; Hjertberg, T.; Nordstierna, L.; Prieto, O.; Müller, C., Orange is the new white: rapid curing of an ethylene-glycidyl methacrylate copolymer with a Ti-bisphenolate type catalyst. *Polym. Chem.* **2018,** *9*, 1710-1718.

112. Mauri, M.; Tran, N.; Prieto, O.; Hjertberg, T.; Müller, C., Crosslinking of an ethylene-glycidyl methacrylate copolymer with amine click chemistry. *Polymer* **2017,** *111*, 27-35.

113. He, J.; Zhou, Y., Progress in Eco-friendly High Voltage Cable Insulation Material. *IEEE Trans. Dielectr. Electr. Insul.* **2018**, 11-16.

114. Zha, J.-W.; Wu, Y.-H.; Wang, S.-J.; Wu, D.-H.; Yan, H.-D.; Dang, Z.-M., Improvement of Space Charge Suppression of Polypropylene for Potential Application in HVDC Cables. *IEEE Trans. Dielectr. Electr. Insul.* **2016,** *23*, 2337-2343.

115. J. Z. Lu; Q. Wu; H. S. McNabb, J., Chemical coupling in wood fiber and polymer composites: a review of coupling agents and treatments. *Wood Fibre Sci.* **2000,** *32*, 88-104.

116. Yin, S.; Tuladhar, R.; Shi, F.; Shanks, R. A.; Combe, M.; Collister, T., Mechanical reprocessing of polyolefin waste: A review. *Polym. Eng. Sci.* **2015,** *55*, 2899-2909.

117. Sclavons, M.; Franquinet, P.; Carlier, V.; Verfaillie, G.; Fallais, I.; Legras, R.; Laurent, M.; Thyrion, F. C., Quantification of the maleic anhydride grafted onto polypropylene by chemical and viscosimetric titrations, and FTIR spectroscopy. *Polymer* **2000,** *41*, 1989-1999.

118. Hu, Y.; Shang, Q.; Wang, C.; Feng, G.; Liu, C.; Xu, F.; Zhou, Y., Renewable epoxidized cardanol-based acrylate as a reactive diluent for UV-curable resins. *Polym. Adv. Technol.* **2018,** *29*, 1852-1860.

119. Kanehashi, S.; Yokoyama, K.; Masuda, R.; Kidesaki, T.; Nagai, K.; Miyakoshi, T., Preparation and characterization of cardanol-based epoxy resin for coating at room temperature curing. *J. Appl. Polym. Sci.* **2013,** *130*, 2468-2478.

120. Tuohedi, N.; Wang, Q., Preparation and Evaluation of Epoxy Resin Prepared from the Liquefied Product of Cotton Stalk. *Processes* **2021,** *9*, 1417.

121. Setz, S.; Stricker, F.; Kressler, J.; Duschek, T.; Mülhaupt, R., Morphology and mechanical properties of blends of isotactic or syndiotactic polypropylene with SEBS block copolymers. *J. Appl. Polym. Sci.* **1996,** *59*, 1117-1128.

122. Abreu, F. O. M. S.; Forte, M. M. C.; Liberman, S. A., SBS and SEBS block copolymers as impact modifiers for polypropylene compounds. *J. Appl. Polym. Sci.* **2005,** *95*, 254-263.

123. Gupta, A. K.; Purwar, S. N., Studies on binary and ternary blends of polypropylene with SEBS, PS, and HDPE. II. Tensile and impact properties. *J. Appl. Polym. Sci.* **1985,** *30*, 1799-1814.

124. Flaris, V.; Wasiak, A.; Wenig, W., The effect of compatibilizers on the morphology of isotactic polypropylene/linear low-density polyethylene blends. *J. Mater. Sci.* **1993,** *28*, 1685-1688.

Paper I

Recyclable Polyethylene Insulation via Reactive Compounding with a Maleic Anhydride-grafted Polypropylene

ACS Applied Polymer Materials

Paper II

High-temperature creep resistant ternary blends based on polyethylene and polypropylene for thermoplastic power cable insulation

Journal of Polymer Science

Paper III

Highly insulating thermoplastic blends comprising a styrenic copolymer for direct current power cable insulation

Manuscript

Paper IV

Highly Insulating Thermoplastic Nanocomposites based on a Polyolefin Ternary Blend for HVDC Power Cables

Manuscript